## **GEOSPHERE**

**GEOSPHERE** 

https://doi.org/10.1130/GES02435.1

16 figures; 1 table; 1 set of supplemental files

CORRESPONDENCE: wkallen@arizona.edu

CITATION: Allen, W.K., Ridgway, K.D., Benowitz, J.A., Waldien, T.S., Roeske, S.M., Fitzgerald, P.G., and Gillis, R.J., 2022, Neogene sedimentary record of the evolution of a translated strike-slip basin along the Denali fault system: Implications for timing of displacement, composite basin development, and regional tectonics of southern Alaska: Geosphere https://doi.org/10.1130/GES02435.1.

Science Editor: Andrea Hampel
Guest Associate Editor: Julie Dumoulin

Received 15 March 2021 Revision received 12 June 2021 Accepted 17 September 2021

First published online 8 February 2022





This paper is published under the terms of the CC-BY-NC license.

© 2022 The Authors

# Neogene sedimentary record of the evolution of a translated strike-slip basin along the Denali fault system: Implications for timing of displacement, composite basin development, and regional tectonics of southern Alaska

Wai K. Allen<sup>1,\*</sup>, Kenneth D. Ridgway<sup>1</sup>, J.A. Benowitz<sup>2</sup>, T.S. Waldien<sup>3</sup>, S.M. Roeske<sup>3</sup>, P.G. Fitzgerald<sup>4</sup>, and R.J. Gillis<sup>5</sup>

- Department of Earth, Atmospheric, and Planetary Sciences, Purdue University, 550 Stadium Mall Drive, West Lafayette, Indiana 47907, USA
- <sup>2</sup>Geophysical Institute and Geochronology Laboratory, University of Alaska-Fairbanks, 900 Yukon Drive, Fairbanks, Alaska 99775, USA
- 3Department of Earth and Planetary Sciences, University of California-Davis, 2119 Earth and Physical Sciences, One Shields Avenue, Davis, California 95616, USA
- <sup>4</sup>Department of Earth Sciences, Syracuse University, 204 Heroy Geology Laboratory, Syracuse, New York 13244, USA
- <sup>5</sup>Alaska Division of Geological & Geophysical Surveys, 3354 College Road, Fairbanks, Alaska 99709-3707, USA

## **ABSTRACT**

Analysis of the late Miocene to Holocene McCallum sedimentary basin, located along the south side of the eastern Denali fault system, provides a better understanding of strike-slip basin evolution, timing of displacement on the Denali fault, and tectonics of the southern Alaska convergent margin. Analysis of the McCallum basin utilizing measured stratigraphic sections, lithofacies analyses, and 40Ar/39Ar tephra ages documented a 564-m-thick, two-member stratigraphy. Fine-grained, lacustrine-dominated environments characterized deposition of the lower member, and coarse-grained, stream-dominated alluvial-fan environments characterized deposition of the upper member. The <sup>40</sup>Ar/<sup>39</sup>Ar dating of tephras indicated that the lower member was deposited from 6.1 to 5.0 Ma, and the upper member was deposited from 5.0 to 3.8 Ma. Our stratigraphic analysis of the McCallum basin illuminates the development of a composite strike-slip basin, with the deposition of the lower member occurring along a transtensional fault section, and deposition of the upper member occurring along a transpressional fault section. This change in depositional and tectonic settings is interpreted to reflect ~79-90 km of transport of the basin along the Denali fault system based on Pleistocene-Holocene slip rates. Previous studies of the timing of Cenozoic displacement on the Denali fault system utilizing sedimentary records emphasized a Paleogene component; our findings, however, also require a significant Neogene component. Neogene strike-slip displacement and basin development along the Denali fault system were broadly coeval with development of high topography and related clastic wedges across southern Alaska in response to flat slab subduction of the Yakutat microplate.

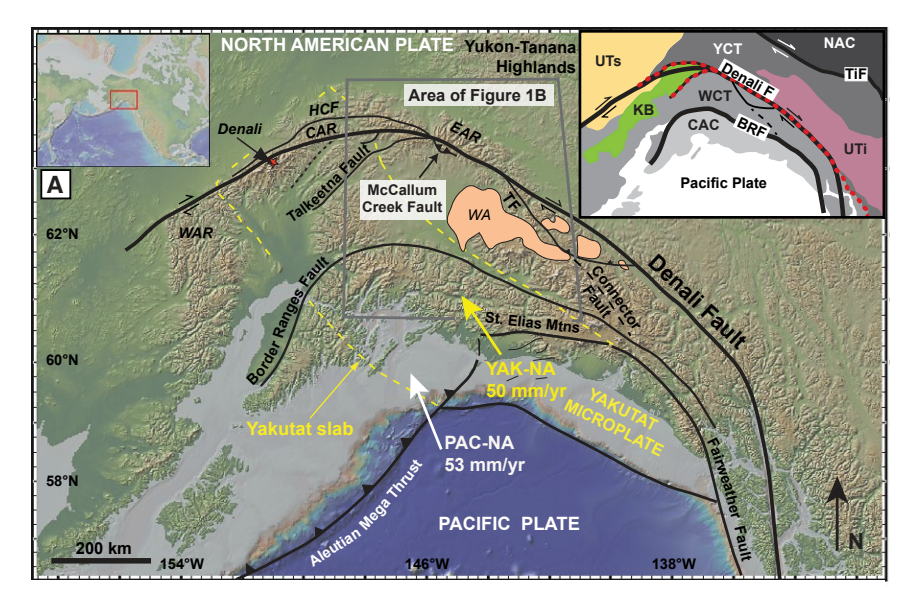
#### ■ INTRODUCTION

The southern Alaska convergent margin was formed by subduction of oceanic crust and accompanying island arcs, spreading ridges, and oceanic plateaus since at least the Jurassic, and this process continues to the present (Fig. 1A; Plafker and Berg, 1994; Nokleberg et al., 1994; Ridgway et al., 2007a). In response to this subduction, the upper plate of this convergent margin contains a rich record of Mesozoic to Cenozoic deformation, exhumation, and basin development (Trop and Ridgway, 2007). Oligocene to ongoing flat slab subduction of the Yakutat microplate, an oceanic plateau, is the most recent phase of this ongoing process (Fig. 1A; Elliott et al., 2010; Finzel et al., 2011; Worthington et al., 2012). Continental strike-slip faults distributed throughout southern and central Alaska accommodate a component of Yakutat–North America convergence, with the Denali fault being the largest active strike-slip system (Fig. 1A; Haeussler et al., 2017a).

In the Alaska Range, late Oligocene to present-day deformation, exhumation, and basin formation along the Denali fault system have been identified in previous studies (Fitzgerald et al., 1993, 1995; Ridgway et al., 2002, 2007b; Trop and Ridgway, 2007; Benowitz et al., 2011). An understudied part of the sedimentary record of deformation in the Alaska Range is the thrust systems and related sedimentary basins located along the south side of the central and eastern Denali fault system (e.g., Fitzgerald et al., 2014; Riccio et al., 2014; Haeussler et al., 2017b; Trop et al., 2019). Our study focused on the Neogene strata of the McCallum formation in the McCallum basin, located 10 km south of the Denali fault in the eastern Alaska Range and presently exposed mainly in the footwall of a southwest-verging thrust system (McCallum Creek fault labeled on Fig. 1A). Neogene strata of the McCallum basin provide an exceptional record of depositional and tectonic processes along the Denali fault system because these strata are deformed, are well exposed, and contain abundant tephras that allow for establishment of a chronostratigraphic framework. Our data sets

Wai Allen https://orcid.org/0000-0002-6624-0862

<sup>\*</sup>Current affiliation: Department of Geosciences, University of Arizona, 1040 E. 4th Street, Tucson, Arizona 85721, USA



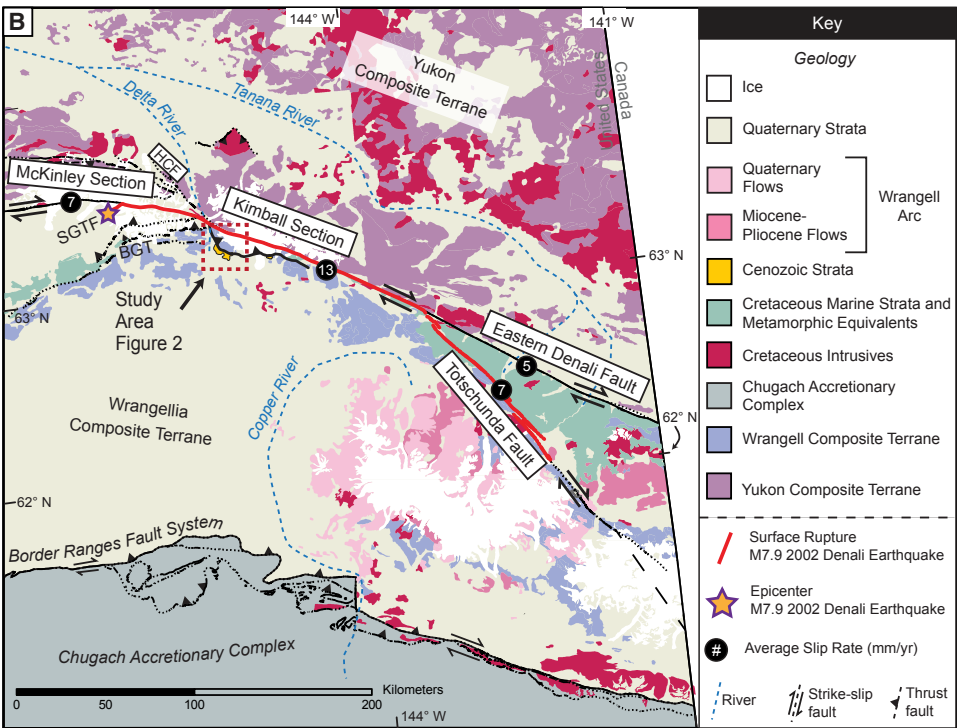


Figure 1. (A) Regional digital elevation model of southern Alaska and adjacent parts of Canada showing the Denali fault system and other major structural elements (from GeoMapApp (www.marinegeo.org/geomapapp; Ryan et al., 2009), CAR-central Alaska Range; EAR-eastern Alaska Range; HCF-Hines Creek fault; TF-Totschunda fault; WA-Wrangell arc; WAR-western Alaska Range. Pacific-North American (PAC-NA) and Yakutat microplate-North American (YAK-NA) motion vectors are summarized from Fletcher and Freymueller (2003); Eberhart-Phillips et al. (2006); Cross and Freymueller (2008); Freymueller et al. (2008); Fuis et al. (2008); and Haeussler (2008). Location of Denali is denoted with a red star. Gray rectangle marks location of part B centered on the eastern Alaska Range. Top-left inset is the geographic location map of the study region. Top-right inset shows configuration of major geologic terranes. Abbreviations: NAC-North American continent, YCT-Yukon composite terrane, WCT-Wrangellia composite terrane, CAC-Chugach accretionary complex, TiF-Tintina fault, BRF-Border Ranges fault, UTi-undifferentiated terranes and igneous rocks, UTs-undifferentiated terranes and sedimentary rocks, KB-Kahiltna Basin, and red dotted line-Mesozoic suture zone between continental (YCT) and oceanic (WCT) terranes (after Brennan et al., 2011; Trop and Ridgway, 2007). (B) Generalized geologic map showing major rock types and terranes in the eastern Alaska Range. Geology is derived from Wilson et al. (2015). The 341 km surface rupture of the M 7.9 Denali earthquake is outlined by the red line (from Haeussler, 2009). Pleistocene-Holocene slip rates along major sections of the Denali fault are annotated based on previous work by Haeussler et al. (2017a). Red dashed box indicates study location. Abbreviations: BGT-Broxson Gulch thrust: SGTF-Susitna Glacier thrust fault: HCF-Hines Creek fault. Figure is adapted from Fitzgerald et al. (2014) and Trop et al. (2019).

consisted of detailed measured stratigraphic sections, <sup>40</sup>Ar/<sup>39</sup>Ar geochronology of tephras, and structural observations. We then integrated our findings to reconstruct the type and timing of depositional systems, and the changes in the tectonic configuration of the basin through time. Our results provide new information on the geomorphic, depositional, and basinal responses to strikeslip displacement along this part of the Denali fault system since ca. 6.1 Ma. Prior to our study, the stratigraphic, depositional, and tectonic framework of the McCallum basin had not been investigated. The regional tectonic significance of the McCallum basin on the south side of the Denali fault has only been addressed in a preliminary manner by the regional synthesis of Ridgway et al. (2002). The Neogene sedimentary record contained in the McCallum basin is critical for a better understanding of the more recent strike-slip displacement history, potential societal geohazards, evolution of the Denali fault system, and regional tectonics of southern Alaska.

Previous studies of strike-slip displacement along the Denali fault system have focused mainly on offset Jurassic-Cretaceous markers across the fault (Eisbacher, 1976; Nokleberg et al., 1985; Lowey, 1998; Fasulo et al., 2020), and Eocene-Oligocene strike-slip basin records (Ridgway and DeCelles, 1993; Ridgway et al., 1995, 1999, 2000). Our study adds to several recent studies that are defining a significant component of Neogene deformation and strikeslip displacement along the eastern Denali fault system (Waldien et al., 2018; Trop et al., 2019). Results of our study also have broader implications for the development of sedimentary basins along strike-slip fault systems. The pioneering work by Crowell et al. (1982) and Mann et al. (1983) established the conceptual framework for development of pull-apart basins that form in mainly transtensional settings. Subsequent research established an extensive body of literature on different types of strike-slip basins (see excellent global review by Mann, 2007). A less well studied type is transpressional basins forming along zones of crustal shortening; some exceptions include Schneider et al. (1996) Cowgill et al. (2004), and Barnes et al. (2005). The strata of the McCallum basin are especially instructive in terms of strike-slip basin development because we interpret these strata to record initial deposition along a transtensional fault section followed by subsequent transport of the basin into a transpressional section of the Denali fault system. We refer to these types of strike-slip basins - basins that record translation along fault sections with different deformational boundary conditions—as composite basins. Composite strike-slip basins should be expected along other strike-slip fault systems with geometric complexity and significant displacement histories, but, to our knowledge, the sedimentary record of these basins has not been well described in the literature.

## ■ REGIONAL GEOLOGIC SETTING AND PREVIOUS WORK

## Geologic Setting of the Denali Fault System and Eastern Alaska Range

The Denali fault is an active dextral strike-slip fault system that extends for more than 2000 km across southern Alaska and northwestern British Columbia

(Fig. 1A; St. Amand, 1957; Grantz, 1966; Stout and Chase, 1980; Dodds, 1992). In south-central Alaska, the fault system is part of a diffuse Mesozoic collisional boundary between Proterozoic(?)-Paleozoic continental margin rocks of the Yukon composite terrane and Paleozoic-Mesozoic oceanic rocks of the Wrangellia composite terrane, with Jurassic-Cretaceous marine sedimentary strata exposed between the terranes (Fig. 1B; Nokleberg et al., 1994; Ridgway et al., 2002; Brennan et al., 2011; Trop et al., 2019; Romero et al., 2020; Waldien et al., 2021). In the region of the study area, the Denali fault system consists of four major sections, and we employ the following terminology to delineate the sections as shown in Figure 1B. The McKinley section extends westward from the junction with the Hines Creek fault (HCF in Fig. 1B). The Kimball section extends from the junction of the Hines Creek fault to the junction with the Totschunda fault (Fig. 1B). At the eastern end of the Kimball section, the fault splays into the eastern Denali fault and the Totschunda fault. We informally refer to the topography associated with the Denali fault system between the headwaters of the Delta River and the Alaska-Canada border as the eastern Alaska Range (Fig. 1B).

Estimates of strike-slip displacement along the Denali fault system vary from tens to hundreds of kilometers based on correlation of variably offset geologic features. Along the eastern and central Denali fault, ~370-450 km of post-Cretaceous strike-slip displacement is estimated based on correlation of offset Jurassic-Cretaceous marine strata (Eisbacher, 1976; Lowey et al., 1998; Fasulo et al., 2020). Nokleberg et al. (1985) estimated 400 km of post-57 Ma strike-slip displacement based on correlation of offset metamorphic belts and intrusive rocks. Also, along the McKinley section, Trop et al. (2019) estimated 150 km of dextral strike-slip displacement of ca. 29 Ma strata based on provenance data. Reed and Lanphere (1974), in contrast, interpreted 38 km of post-38 Ma displacement along the McKinley section based on offset plutons. A more recent study, however, interpreted these two plutons as being unrelated, not offset halves of the same pluton, thus questioning this displacement estimate (Regan et al., 2020). More recent displacement records are based on cosmogenic exposure dating of offset geomorphic features. Pleistocene-Holocene slip rates based on this approach indicate slip rates between ~5 and 13 mm/yr along the Denali fault sections (black circles in Fig. 1B; Matmon et al., 2006; Mériaux et al., 2009; Haeussler et al., 2017a; Marechal et al., 2018).

The Totschunda fault is a dextral strike-slip fault that extends at least 200 km southeastward from its junction with the Denali fault (Fig. 1B; Richter and Matson, 1971; Schwartz et al., 2012). The displacement history along this structure is unclear. In some studies, the Totschunda fault was thought to be a very young structure, in the age range of 2 Ma (Richter and Matson, 1971; Bemis et al., 2015). More recent studies based on a dike intrusion within the Totschunda fault zone suggest that this fault had to have been active since at least ca. 29 Ma (Brueseke et al., 2019). Another recent study has estimated ~85 km of displacement since 18 Ma based on offset intrusive rocks of the Wrangell arc along the Totschunda fault (Berkelhammer et al., 2019). That estimate is consistent with an estimated minimum of 75 km of displacement on the Totschunda fault based on offset marine strata of the Jurassic–Cretaceous Nutzotin Mountain sequence (Fasulo et al., 2020).

## Geologic Setting and Previous Work on the McCallum Basin

Series of generally south-verging thrust faults have been mapped along the south side of the Kimball and McKinley sections of the Denali fault (Fig. 1B; e.g., Bond, 1976; Stout, 1976; Ridgway et al., 2002; Waldien et al., 2018, 2021). In our study area, the interior thrust sheets, directly south of the Denali fault, juxtapose mainly Paleozoic igneous rocks with Mesozoic igneous rocks (Fig. 2; Nokleberg et al., 1992a, 1992b, 2015). The exterior thrust sheets carry Paleozoic and Mesozoic igneous rocks, Eocene volcanic strata, and locally Upper Miocene to Pliocene sedimentary strata. The McCallum Creek fault is the southernmost-exposed thrust fault in this south-verging series of faults (Fig. 2). Our study area, the northeastern part of the McCallum basin, is best exposed in the footwall of the McCallum Creek thrust fault (Fig. 2).

Exposures of the McCallum basin crop out in a northwest-southeast-trending belt along the southern flank of the eastern Alaska Range (Fig. 2). Here, Upper Miocene to Holocene sedimentary and minor volcanic strata are well exposed along both Phelan and McCallum Creeks; we informally refer to these strata as the McCallum formation. Previous gravity and seismic geophysical studies have defined the basin geometry as 28 km long (northwest trending) and 18 km wide with basinal strata that are ~1.5 km thick in the subsurface (Morin and Glen, 2003; Brocher et al., 2004). Previous geologic work in the McCallum basin was limited to focused geologic mapping (Hanson, 1963; Bond, 1976; Stout, 1976) and regional compilations (Ridgway et al., 2002; Nokleberg et al., 1982, 1992a, 1992b, 2015). A more recent detailed structural and mapping study by Waldien et al. (2018) documented the geometry of the thrust system adjacent to the McCallum basin as part of a strike-slip flower structure related to partitioned transpression along the Kimball section of the Denali fault. Apatite fission-track cooling ages indicate that slip on the master McCallum Creek fault resulted in as much as ~4.8 km of bedrock exhumation since ca. 6 Ma (Waldien et al., 2018). The age of the strata of the McCallum formation has only received limited attention in prior studies. Previous work determining the age of these strata was based on K-Ar hornblende and K-Ar plagioclase ages (n = 10) from tephra beds with isochron ages that ranged from 7.45 to 4.78 Ma (Turner et al., 1980; Kunk, 1995). These initial K-Ar studies did not place dated samples into a stratigraphic framework.

### DATA

## Stratigraphic Framework of the McCallum Formation

We defined a two-member stratigraphy for the McCallum formation based on 11 measured stratigraphic sections, lithofacies analyses, and 40 Ar/39 Ar dating

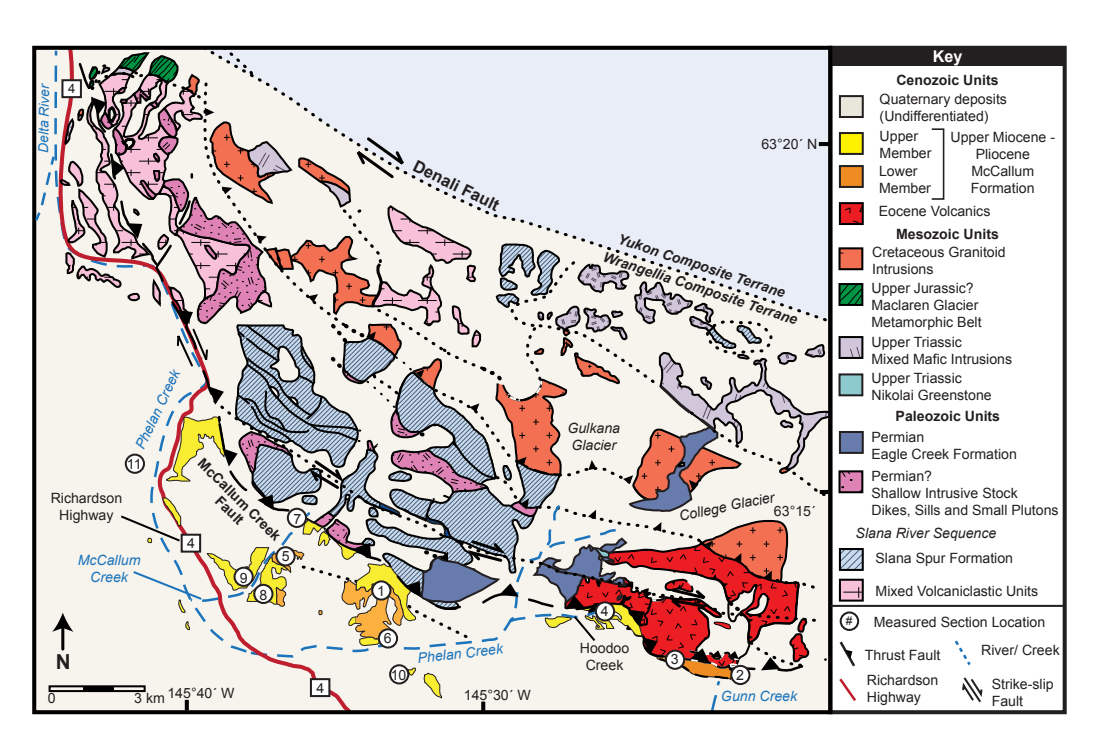


Figure 2. Simplified geologic map showing locations of measured stratigraphic sections from this study denoted by circled numerical symbols that are discussed in the text. We refer to the extent of exposures of Neogene strata in the footwall of the McCallum Creek fault as the McCallum formation within the McCallum basin. Geologic units are adapted from maps by Ridgway et al. (2002), Nokleberg et al. (2015), Waldien (2015), and Waldien et al. (2018).

of tephras (Figs. 2 and 3). Tephra dates were determined as part of our study at eight of the 11 measured stratigraphic sections (Figs. 3, 4, and 5). The <sup>40</sup>Ar/<sup>39</sup>Ar geochronologic methods employed are described in detail in the following section. We used lithofacies correlation, tephra dates, and physical correlation between individual beds to construct a chronostratigraphic composite section of the McCallum formation that has an overall thickness of 564 m (Fig. 6A). Measured sections with the largest stratigraphic thickness were selected for construction of the composite section and are highlighted with red boxes in Figure 3. The lower member has a conservatively estimated stratigraphic thickness of 181.5 m, which was derived from the measured section 2 because it was the longest continuous section for the lower member (Fig. 3). We chose this conservative approach based on the limited exposures and an average distance of ~2 km between geographic locations of measured sections that characterize the lower member (Fig. 2). Our estimated stratigraphic thickness

of 383 m for the upper member was derived from a combination of measured sections 8, 9, and 10 (Fig. 3). Measured sections 8 and 9 are located within less than a 0.5 km distance of each other and are along strike of each other, with the projection of measured section 8 below measured section 9 (Figs. 2 and 3). The stratigraphic thickness of measured section 10 was added to the estimated thickness of the upper member to account for the presence of the youngest dated tephra (3.8 Ma).

## <sup>40</sup>Ar/<sup>39</sup>Ar Geochronology of Tephras

We identified 24 tephra beds during our study of the McCallum formation. Eight tephra samples were collected for 40Ar/39Ar dating in the context of measured sections to construct a chronostratigraphic framework for the McCallum

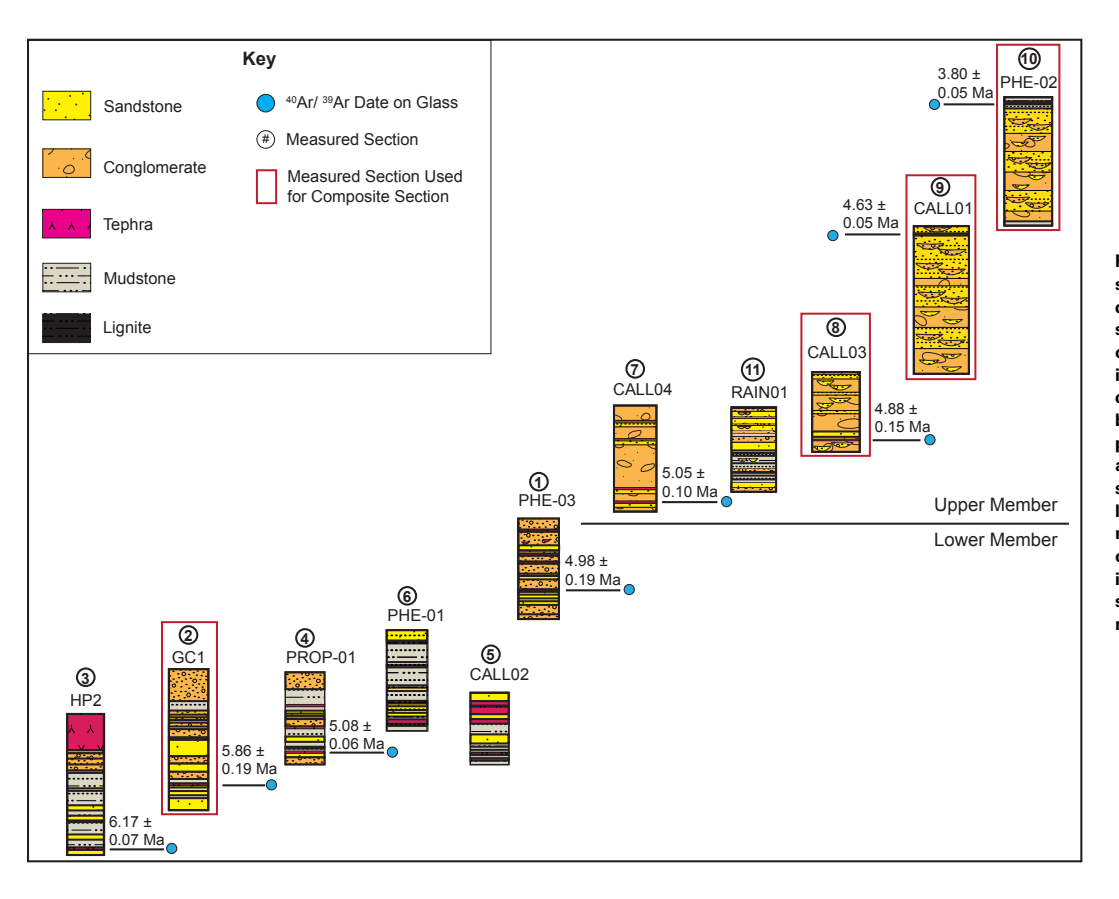


Figure 3. Correlation diagram of individual measured stratigraphic sections and tephra ages documented for the McCallum formation in the study area. The composite stratigraphic section of the McCallum formation shown in Figure 6A is based on correlation of lithofacies, 40Ar/39Ar dates of tephra samples, physical correlation between individual beds, and geologic mapping between individual sections. Red boxes around measured sections indicate specific sections used for estimated thicknesses of the lower and upper member of the McCallum formation. See Figure 2 for geographic locations of individual measured stratigraphic sections in the McCallum basin and Figures 7 and 10 for stratigraphic thicknesses in detailed individual measured sections.

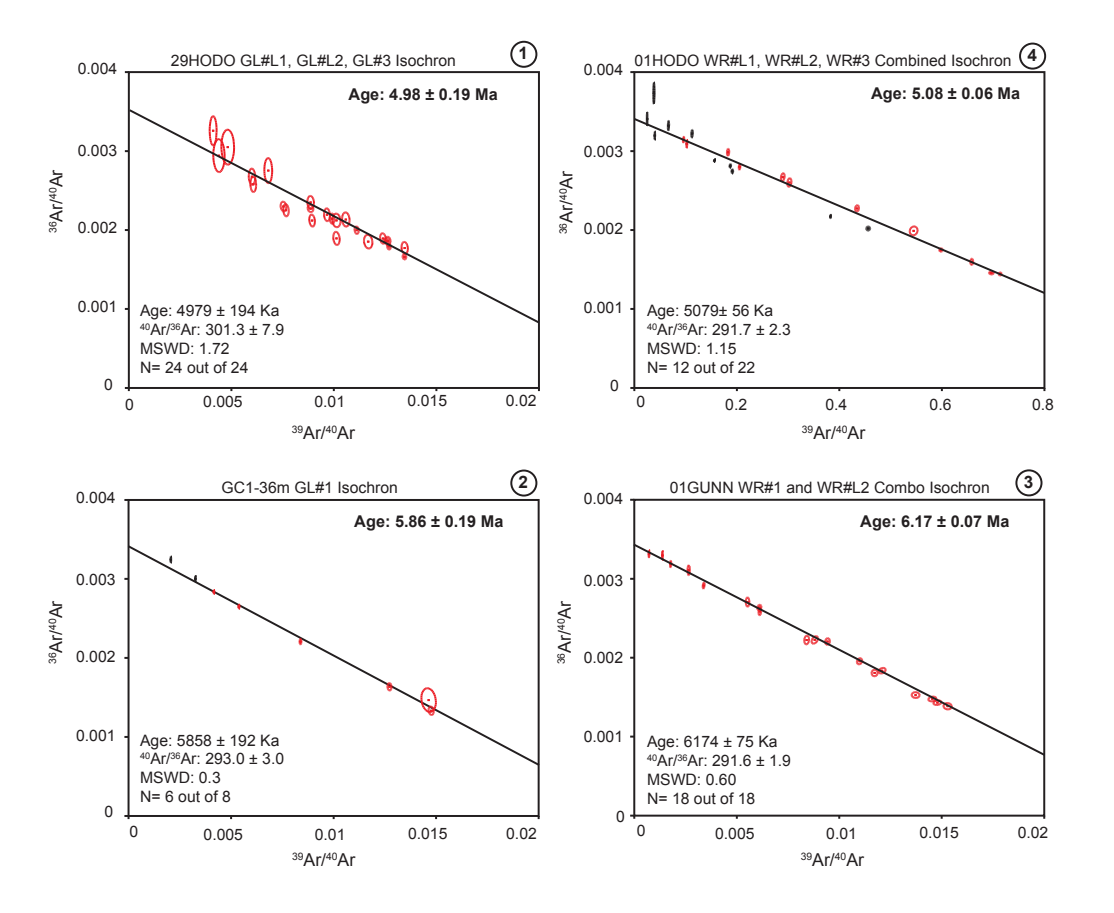


Figure 4. Inverse isochron diagrams for volcanic glass from four tephras sampled from the lower member of the McCallum formation. Circled numbers in headings correspond to samples collected from measured section locations 1. 2, 3, and 4 in Figure 2, which can be viewed in stratigraphic context in Figure 3. Isochron ages were calculated from <sup>36</sup>Ar/<sup>40</sup>Ar vs. <sup>39</sup>Ar/<sup>40</sup>Ar ratios recorded during each individual heating step. Steps selected for isochron age determination are shown in red ellipses, and steps not selected are in black ellipses. Total N value summarizes the number of steps selected for each sample. The mean square of weighted deviates (MSWD) values range from 1.72 to 0.3 for the samples. Samples with multiple aliquots are denoted with glass (GL) or whole-rock (WR) notation and are reported as combined isochron ages. The oldest dated tephra is 6.17 ± 0.07 Ma, and the voungest dated tephra is 4.98 ± 0.19 Ma from the lower member.

formation (Figs. 3, 4, and 5; Table S1 in the Supplemental Material¹). Tephra samples typically consisted of ~90% volcanic glass and ~10% feldspar. Individual volcanic glass grains (18–24 grains per sample) were selected for multigrain analysis using 40Ar/39Ar geochronology. These samples were processed at the Geochronology Facility at the University of Alaska–Fairbanks to extract 99% pure volcanic glass separates for each sample. Each separate was examined under an optical microscope to confirm identification and purity. Separates were irradiated at McMaster University Nuclear Reactor in Hamilton, Ontario, Canada. Individual grains were then laser step-heated from relatively low temperatures until reaching fusion temperatures using a 6W argon-ion laser (e.g., Śliwiński et al., 2012). For each step, isotopic ratios of Ar were analyzed

using a VG3600 mass spectrometer that produced a spectrum of ages based on individual steps. A more detailed description of this method can be found in Śliwiński et al. (2012) and Benowitz et al. (2011). The <sup>40</sup>Ar/<sup>39</sup>Ar analyses were determined by coauthor Jeff A. Benowitz at the Geochronology Facility at the University of Alaska–Fairbanks. Results of these analyses are reported as inverse isochron ages with a range of mean square of weighted deviation (MSWD) values of 0.3–2.14 (Figs. 4 and 5). Inverse isochron ages were calculated from an inverse isochron diagram of <sup>36</sup>Ar/<sup>40</sup>Ar versus <sup>39</sup>Ar/<sup>40</sup>Ar isotopic ratios recorded during each individual heating step (Roddick, 1978; Roddick et al., 1980; Benowitz et al., 2011). Recent work has demonstrated that <sup>40</sup>Ar/<sup>39</sup>Ar dating of volcanic glass can produce robust and reproducible results (Cogliati et al., 2021). The robustness of <sup>40</sup>Ar/<sup>39</sup>Ar dating of volcanic glass (tephra dating) and hence potential alteration can be evaluated by multi-aliquot dating. We utilized <sup>40</sup>Ar/<sup>39</sup>Ar multigrain analyses of one to three aliquots of glass for each tephra sample. For samples where two or more analyses were performed,

<sup>&</sup>lt;sup>1</sup>Supplemental Material. Ar/Ar geochronologic and U-Pb detrital zircon geochronologic ages. Please visit <a href="https://doi.org/10.1130/GEOS.S.16892557">https://doi.org/10.1130/GEOS.S.16892557</a> to access the supplemental material, and contact editing @geosociety.org with any questions.

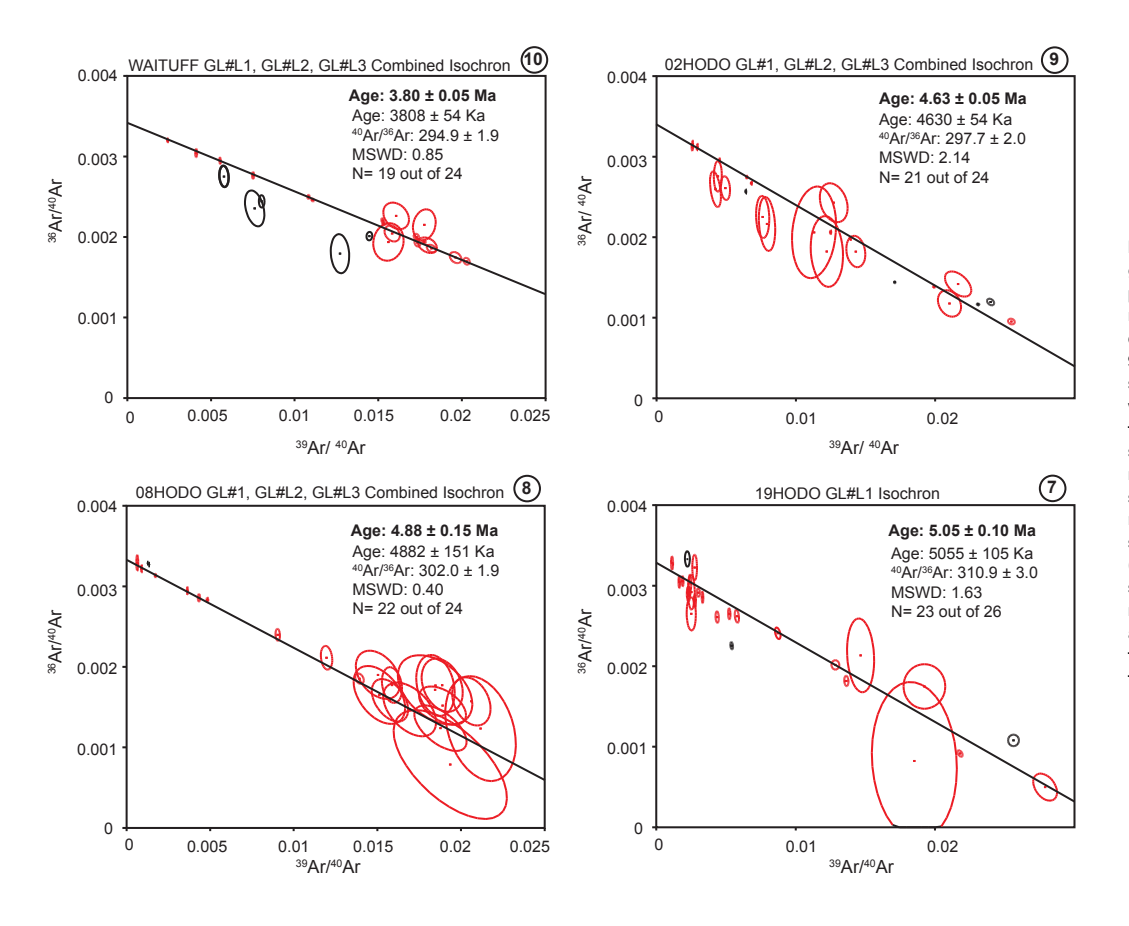


Figure 5. Inverse isochron diagrams for volcanic glass from four tephras sampled from the upper member of the McCallum formation. Circled numbers in headings correspond to samples collected from measured section locations 7, 8, 9, and 10 in Figure 2, which can be viewed in stratigraphic context in Figure 3. Isochron ages were calculated from <sup>36</sup>Ar/<sup>40</sup>Ar vs. <sup>39</sup>Ar/<sup>40</sup>Ar ratios recorded during each individual heating step. Steps selected for isochron age determination are shown in red ellipses, and steps not selected are in black ellipses. Total N value summarizes the number of steps selected for each sample. The mean square of weighted deviates (MSWD) values range from 2.14 to 0.4 for the samples. Samples with multiple aliquots are denoted with glass (GL) notation and are reported as combined isochron ages. The oldest dated tephra is 5.05 ± 0.10 Ma, and the youngest dated tephra is 3.80 ± 0.05 Ma for the upper member.

composite isochrons were compiled from the individual analyses. Composite isochrons are a common technique applied in  $^{40}\text{Ar}/^{39}\text{Ar}$  geochronology applications to account for potential excess  $^{40}\text{Ar}$  and to increase overall precision (e.g., Sharp and Renne, 2005; Cassata et al., 2008). Figures 2 and 3 display the stratigraphic positions and geographic locations for individual tephra samples collected for  $^{40}\text{Ar}/^{39}\text{Ar}$  analysis. As shown in Figure 6A, the stratigraphically oldest dated tephra is 6.17  $\pm$  0.07 Ma, and the stratigraphically youngest dated tephra is 3.80  $\pm$  0.05 Ma.

## **Sedimentology and Depositional Systems**

Detailed sedimentologic observations were made while measuring a total of >1.2 km of individual stratigraphic sections on a bed-by-bed basis using a Jacob's staff. Paleoflow indicators were based on measurement of 10

imbricated clasts in a conglomerate bed and are shown in Figure 6A. Clast compositional data from conglomerate were collected by identifying ~100 individual clasts within a delineated rectangular area within individual beds; these data are shown in Figure 6B. Utilizing this data set, we subdivided the McCallum formation into nine main lithofacies that define the depositional systems of the lower and upper members (see summary of lithofacies descriptions and interpretations in Table 1). In the following sections, we describe each of the nine main lithofacies documented in the McCallum formation.

## Stratigraphic Context of the Lower Member

The lower member is characterized by predominantly laminated mudstone, sandstone, and granule to pebble conglomerate, and it has a minimum thickness of 181.5 m (Fig. 6). Tephra and lignite beds are common in the lower

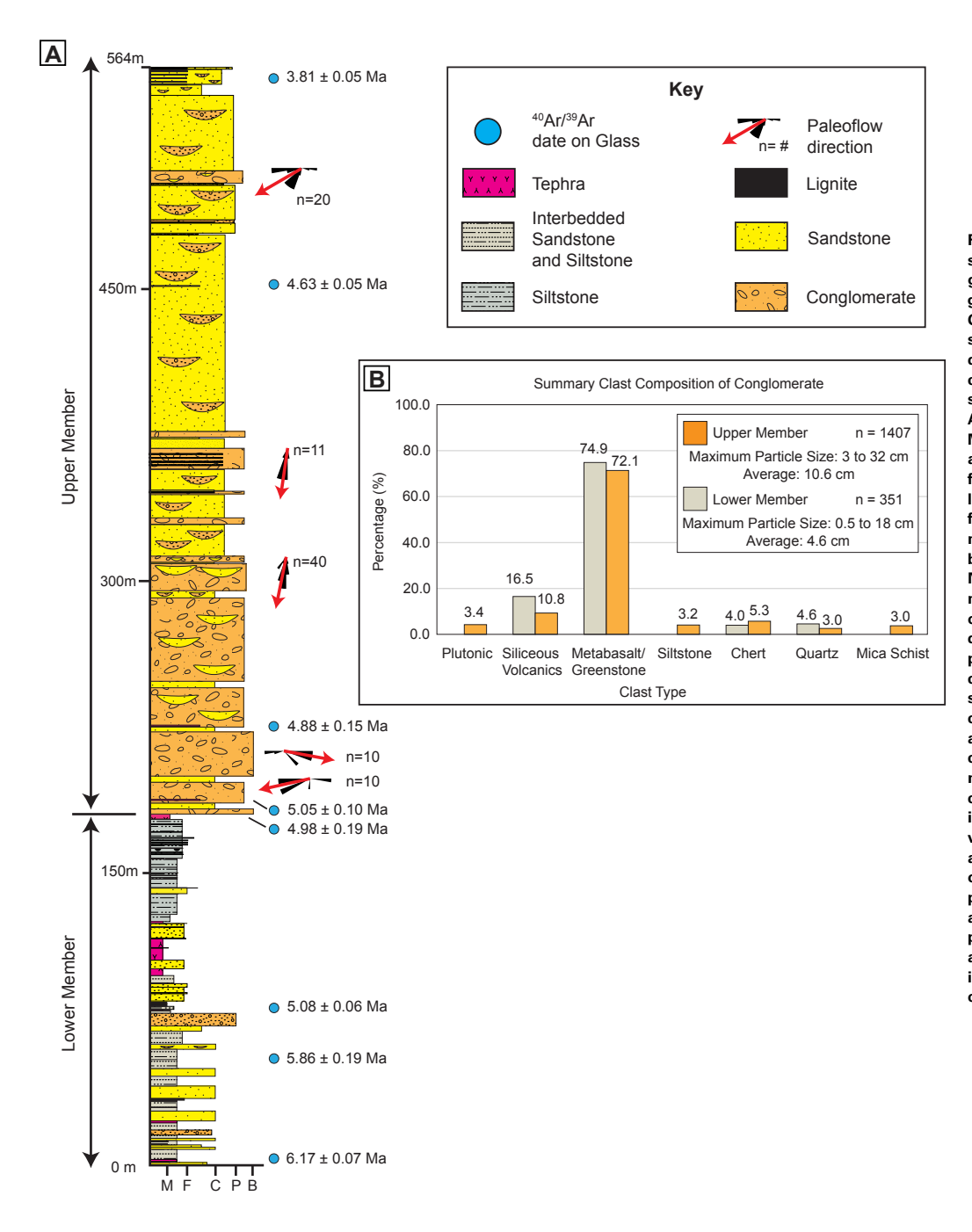


Figure 6. (A) Composite measured stratigraphic section of the McCallum formation showing stratigraphic positions of tephras dated with 40Ar/39Ar geochronology on volcanic glass (blue circles). Grain-size abbreviations: M-clav and silt: F-fine sand, C-coarse sand, P-pebble, B-boulder. Rose diagrams adjacent to the composite section were constructed using the Stereonet 9.5 program designed by Allmendinger et al. (2012) and Cardozo and Allmendinger (2013). Rose petals have a 15° width. Mean paleoflow direction is indicated with a red arrow. (B) Histogram showing clast compositions from the lower and upper members of the McCallum formation. Histogram represents 19 clast counts from seven measured stratigraphic sections and one mapping locality. Numbers above each histogram bar are relative percentages for each clast category. Note discrepancy in n values between the lower member and upper member due to the relative lack of conglomerate in the lower member. Thirty-eight different clast types were identified from hand samples and subsequently grouped into seven general categories: plutonic, siliceous volcanics, basalt, siltstone, chert, quartz, and mica schist. The plutonic category includes granitoid clasts with hornblende and biotite. Mica schist clasts include gray and green color varieties. Siltstone includes black and brown meta-siltstones. Metamorphosed basalt includes chlorite-rich green and black varieties. Chert clasts include black, tan, and green varieties. Siliceous volcanics include yellow, green, tan, black, gray, and white varieties. Note the relative abundance of metabasalt compositions. Average maximum particle size for the lower member is 4.6 cm, with a range of 0.5 cm to 18 cm. The average maximum particle size for the upper member is 10.6 cm, with a range of 32 cm to 3 cm. We interpret the relative increase in particle size to be related to propagation of the thrust system into proximal parts of the basin.

TABLE 1. LITHOFACIES DESCRIPTIONS AND INTERPRETATIONS FOR UPPER MIOCENE-PLIOCENE STRATA OF THE MCCALLUM BASIN

Facies codes	Color, bedding, texture, structures	Facies interpretations
F1	Granule-pebble conglomerate, moderately sorted, and clast-supported, with rounded to subrounded clasts; crudely horizontally stratified and often overlain by sandstone and lignite; most beds are 5.5 m thick.	High-velocity streamflow processes and channel bar migration in proximal stream-dominated alluvial-fan systems (Smith, 1974; Godin, 1991; Sambrook-Smith et al., 2006; Bridge, 2006; Bridge and Lunt, 2009).
F2ab	Medium- to coarse-grained sandstone, normally grades into organic-rich siltstone and tephra (a), commonly contains lignite beds, locally contains horizontal stratification with granule to pebble conglomerate lenses, and has large coalified wood fragments organized in a chaotic manner (b); most beds are 4 m thick and amalgamate to as much as 22 m thick.	Streamflow conditions in broad, sand-rich channelized environments; highly vegetated adjacent floodplains (Nichols and Fisher, 2007; Miall, 2010).
F3	Laminated mudstone interbedded with minor fine-grained sandstone that grades normally into ripple-stratified siltstone-rich beds that contain plant fragments; siltstone beds often grade into laminated mudstone beds; most beds are 6 to 1 m thick. Present in both the lower and upper member.	Low-velocity, suspension settling processes in standing water within lacustrine environments with episodic/seasonal underflow turbidity currents during flood conditions; best preserved in distal basin facies (Sturm and Matter, 1978; Fouch and Dean, 1982; Talbot and Allen, 1996; Schnurrenberger et al., 2003; Ridgway et al., 2007b; Renaut and Gierlowski-Kordesch, 2010).
F4	Laterally continuous volcanic ash deposits at the outcrop scale; contains abundant vesicular and cuspate volcanic glass shards; beds commonly have sharp basal contacts and contain laminations that grade into fine-grained organic-rich layers. Present in both lower member and upper member. Most beds are 1 m thick in the lower member; most beds are 15 cm thick in the upper member.	Air-fall tephra deposited during volcanic eruptions (Smith, 1991).
F5	Lignite horizons interbedded with laminated tephra layers; most beds are 20 cm thick.	Swamps, marshes, wet floodplains; best preserved in distal basin facies (McCabe, 1985).
F6	Clast-supported, boulder-pebble conglomerate, crudely horizontally stratified, with subrounded to angular clasts, locally imbricated; interbedded sandstone locally contains subordinate tephra beds; most beds are 6 m thick but can amalgamate to 22 m thick.	High-velocity, streamflow processes associated with proximal environments of stream-dominated, alluvial-fan systems (Rust and Jones, 1987; Collinson, 1996; Miall, 2010).
F7	Organized, clast-supported, pebble-cobble conglomerate with subordinate lenticular sandstone lenses, horizontally stratified, with subrounded to rounded clasts, imbricated; interbedded with normally graded horizontally stratified sandstone; most beds are 5 m thick.	Bedload transport by tractive currents under hydrodynamically stable flow conditions of longitudinal bars in shallow medial stream-dominated alluvial-fan systems (Collinson, 1996; Lunt and Bridge, 2004; Nichols and Fisher, 2007).
F8	Well-organized, sandy clast-supported conglomerate, and granule-pebble-cobble conglomerate contain subrounded clasts that are often imbricated; interbedded sandstone, commonly contains trough cross-stratification; most beds are 5 m thick.	Bedload transport by tractive current processes; deposition in longitudinal and transverse bars in distal stream-dominated alluvial-fan systems (Ghinassi and lelpi, 2016).
F9	Sandstone with abundant granule-conglomerate lenses; low-angle to horizontal stratification is common; most beds are 5 m thick and amalgamate to as much as 84 m thick.	Midchannel bars with basal lag deposits resulting from sandy bedload channels of medial-distal region of stream-dominated alluvial-fan systems with well-developed sandflats (Collinson, 1996; Nichols and Fisher, 2007; Fisher et al., 2007; Miall, 2010).

member (Fig. 7). The stratigraphically lowest dated tephra in the lower member has a  $^{40}$ Ar/ $^{39}$ Ar age of 6.17  $\pm$  0.07 Ma (measured section 3 in Fig. 7), and the stratigraphically highest dated tephra in the lower member has an age of 4.98  $\pm$  0.19 Ma (measured section 1 in Fig. 7). We informally defined the type section of the lower member as the well exposed strata along Phelan Creek (measured section 6 in Fig. 2; see also Fig. 7).

#### Common Lithofacies of the Lower Member

**Facies 1.** Organized, clast-supported granule to pebble conglomerate with sandstone and liquite.

Description: Facies 1 consists of upward-fining packages of granule to pebble conglomerate that grade into fine- to medium-grained sandstone and

lignite (measured sections 1 and 2 in Fig. 7; see also Fig. 8A). These packages have average thicknesses of 5.5 m, with a range from 1.5 to 16 m. The lower part of the package consists of conglomerate beds with erosive basal contacts. These conglomerate beds are crudely horizontally stratified with average thicknesses of 3.5–5.5 m. Conglomerate clasts are rounded to subrounded and have an average maximum particle size of 4 cm, with a range from 2 to 18 cm (Fig. 8A). The dominant clast type in the conglomerate is metabasalt (greenstone) (Fig. 6B). Sandstone lenses are common in the conglomerate beds. These lenses range in thickness from 30 to 65 cm; locally, these lenses have discontinuous horizons of tephra that range in thickness from 5 to 30 cm. The tops of conglomerate beds are commonly overlain with sandstone containing lignite horizons (Fig. 8A). These overlying sandstone beds are fine-to medium-grained, horizontally stratified beds, and they have average bed thicknesses of 1–6 m. Individual lignite horizons have thicknesses that range

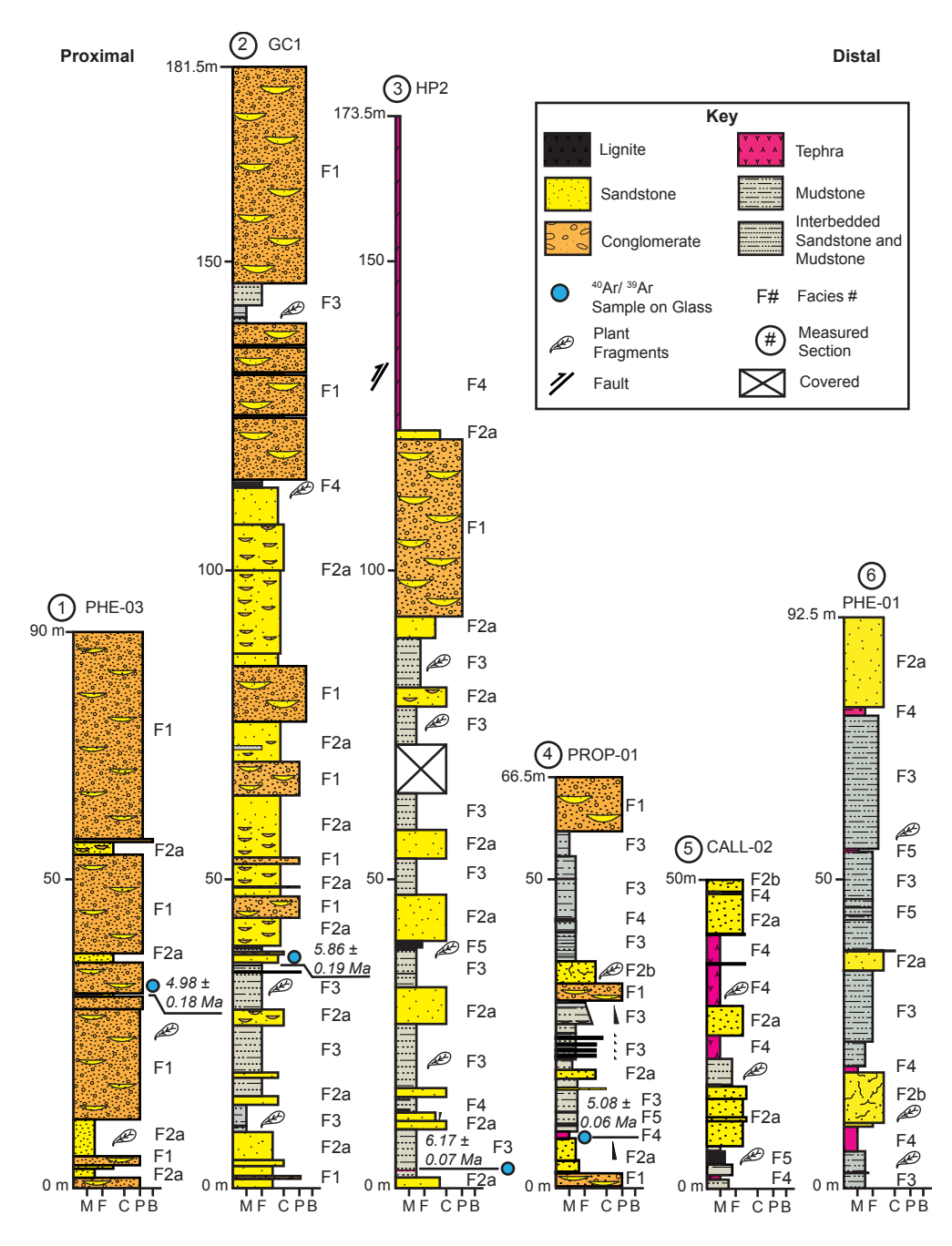


Figure 7. Individual detailed measured sections from the lower member of the McCallum formation showing lithologies, facies type, and stratigraphic positions of tephras dated with <sup>40</sup>Ar/<sup>39</sup>Ar geochronology. Each measured section number correlates with their respective geographic locations in Figure 2. Each facies number correlates with their respective detailed facies description discussed in the text and summarized in Table 1. The relative position of each measured section in this figure represents an interpreted proximal to distal basinal location as discussed in the text. Both measured section and facies numbers also correlate with their location within the interpreted depositional setting for the lower member as shown in Figure 9. See Figure 6 for grainsize abbreviations.

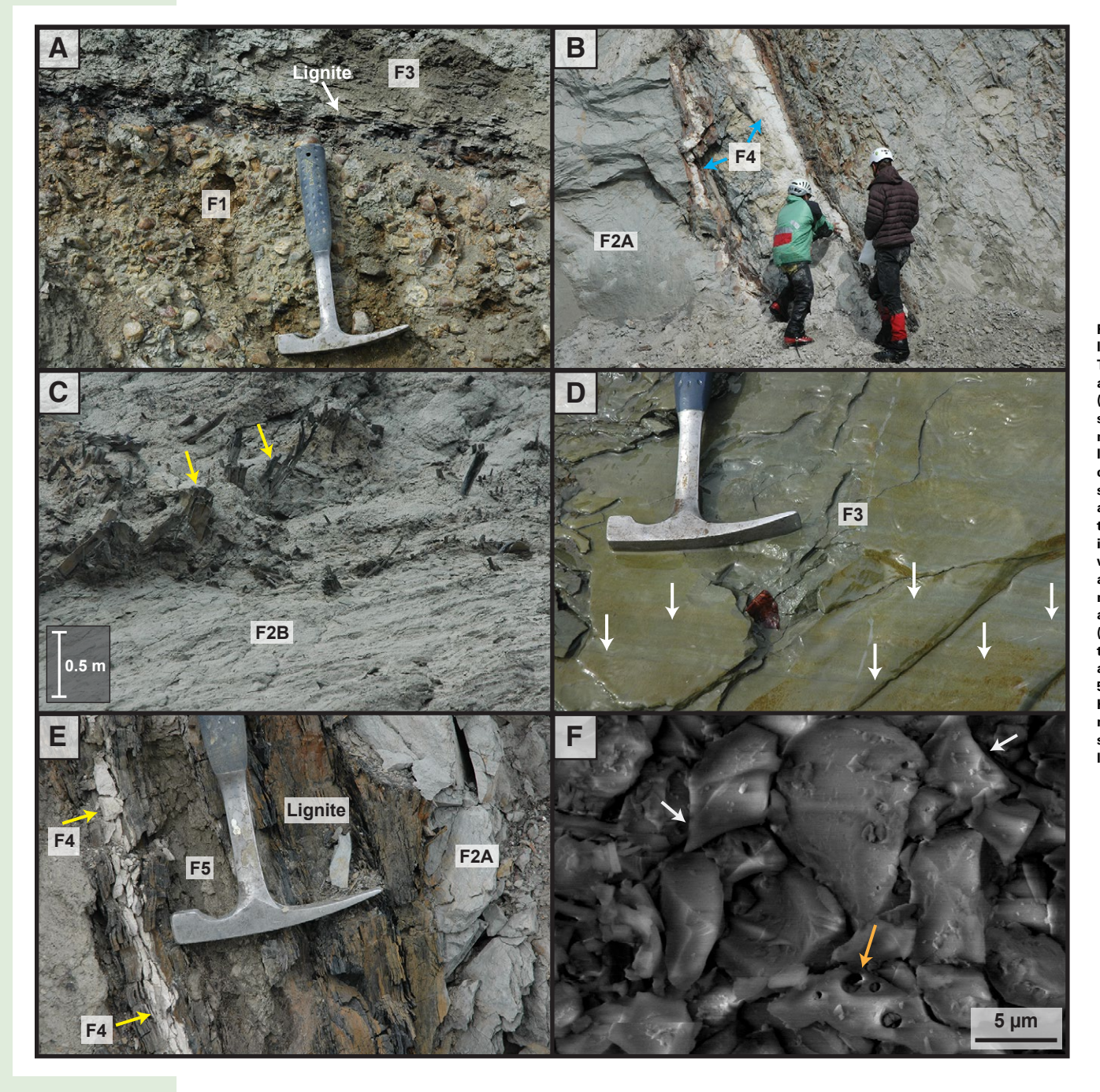


Figure 8. Common lithofacies documented in the lower member of the McCallum formation. See Table 1 for facies codes, lithologic descriptions, and interpretations for individual lithofacies. (A) Facies 1 (F1) consists of organized clastsupported, granule to pebble conglomerate with minor sandstone and siltstone. Note lignite overlying F1. Hammer for scale. (B) Facies 2A (F2A) consists of massive medium- to coarse-grained sandstone that is commonly overlain by lignite and tephra (facies 4; F4). Bedding dips steeply to the right. People for scale. (C) Facies 2B (F2B) is characterized by coarse-grained sandstone with horizons of abundant woody debris (yellow arrows). (D) Facies 3 (F3) consists of laminated mudstone and siltstone. Individual laminae are shown by white arrows. Hammer for scale. (E) Facies 4 (F4) is characterized by laterally continuous volcanic ash layers (yellow arrows) that are commonly interbedded with lignite (facies 5; F5). Bedding is dipping steeply to the right. Hammer head for scale. (F) Scanning electron microscope image of tephra. Note volcanic glass shards with cuspate (white arrows) and vesicular textures (orange arrow).

from 6 to 10 cm. Sandstone beds locally contain granule conglomerate lenses with thicknesses of 50–70 cm, and they often include clasts of lignite. These conglomerate lenses have subrounded to subangular clasts with an average maximum particle size of 2.6 cm and a range from 0.5 to 6 cm. This facies accounts for 31% of the lower member and is best exposed in measured sections 1, 2, and 4 in Figure 7. The conglomerate beds of facies 1 are best developed adjacent to the McCallum Creek fault and grade southward and southwestward into facies 2.

Interpretation: We interpret facies 1 to represent deposition by streamflow processes within migrating channel bar forms. Horizontally stratified, clast-supported conglomerate with erosive basal contacts indicates deposition by bedload transport during high-velocity flows, and the migration of longitudinal bars in channelized systems (Smith, 1974; Sambrook-Smith et al., 2006). The upward-fining packages represent the gradual abandonment of individual channels. During high-flow conditions, vegetated channel bars were quickly buried, preventing oxidation and allowing preservation of organic material that formed the thin lignitic horizons. We interpret sandstone lenses, containing horizontal stratification, as a product of deposition on top of channel bars and along the flanks of bars during waning flow conditions (e.g., Godin, 1991; Bridge, 2006; Bridge and Lunt, 2009). During these low-flow conditions, channel bars were quickly revegetated, based on the occurrence of multiple thin lignite layers directly above the conglomerate (Fig. 8A). The overlying sandstone beds with lignite are interpreted to represent deposition in inactive channels.

**Facies 2.** Massive, medium- to coarse-grained gray sandstone with disarticulated fossilized wood fragments.

Description: We subdivided facies 2 into two types: facies 2A and facies 2B. Facies 2A consists of upward-fining packages of moderately sorted, massive, medium- to coarse-grained gray sandstone interbedded with organic-rich laminated siltstone and tephra (Fig. 8B). Sandstone beds have average thickness of 3.3 m in our measured sections, with a range of thicknesses from 1 to 4.5 m. Individual beds can form amalgamated packages that are up to 22.5 m thick (best exposed in measured section 2 at 100 m in Fig. 7). Sandstone beds are generally massive but locally contain horizontal stratification and trough cross-stratification. These sandstone beds also contain lenses of granule to pebble conglomerate that include lignite fragments. Conglomerate lenses in sandstone beds are ~10 cm thick with granule- to pebble-sized subrounded clasts. These sandstone packages fine upward into organic-rich siltstone beds containing lignite that have bed thicknesses ranging from 20 to 50 cm. Facies 2B has the same general lithologic characteristics of facies 2A but also contains large coalified wood fragments concentrated in specific horizons in a chaotic manner (Fig. 8C). Facies 2B is best exposed in measured sections 4 and 6 in Figure 7. We subdivided facies 2 on our measured sections to make it easier for future researchers to identify these paleo-wood-rich horizons. Facies 2 makes up 29% of the lower member, and it is best exposed in measured sections 2, 4, 5, and 6 in Figure 7. The sandstone beds of facies 2 grade and interfinger basinward into facies 3.

Interpretation: We interpret facies 2 to represent tractive transport of sand in channelized environments. Thick, amalgamated, massive-bedded sandstone packages in this facies suggest to us that these sands were rapidly deposited by turbulent bedload and suspended sediment transport. These are common processes in streamflow conditions associated with multiple-channelized systems (e.g., Nichols and Fisher, 2007; Miall, 2010). We interpret the general lack of sedimentary structures indicative of well-organized bed forms to suggest episodic high-velocity sheet flows during bankfull conditions (facies 2A). During maximum flood conditions, the high-velocity flows are interpreted to have inundated vegetated floodplains. The abundance and high density of disorganized woody detritus and other plant fragments in facies 2B suggest that during flood conditions, vegetation was rapidly incorporated into channels and transported.

**Facies 3.** Laminated mudstone with subordinate sandstone and siltstone with fossilized plant debris.

Description: Facies 3 is characterized by laminated gray mudstone interbedded with minor sandstone and siltstone (Fig. 8D). Laminated mudstone beds have individual bed thicknesses that range from 1 to 6 m. Laminations are defined by subtle changes in grain size and organic detritus content. Fluid escape structures locally disrupt the laminations. Fine- to medium-grained sandstone beds with individual thicknesses that range from 3 to 30 cm commonly have sharp lower contacts with underlying laminated mudstone. Sandstone beds commonly have ripple stratification and grade normally into siltstone beds that are brown in color and rich in mica and organic detritus. Locally, siltstone beds contain climbing ripple stratification, and laminations defined by disarticulated fossilized plant fragments. Siltstone beds grade vertically into thicker-bedded, laminated mudstone. Facies 3 is the most common facies in basinward exposures of the lower member, forming over 34% of the total lithofacies, and is best exposed in measured sections 4 and 6 in Figure 7. The mudstone-rich units of facies 3 are interbedded with facies 4 and 5.

Interpretation: We interpret mudstone of facies 3 to have been deposited mainly through suspension fallout processes common in lacustrine environments (e.g., Renaut and Gierlowski-Kordesch, 2010). Preservation of laminae in the mudstone indicates deposition by low-velocity, suspension-settling processes in standing water (e.g., Talbot and Allen, 1996; Schnurrenberger et al., 2003). The laminations that characterize this facies may represent seasonal varves, such as those reported from lacustrine strata deposited in temperate climates (e.g., Fouch and Dean, 1982; Ridgway et al., 2007b; Renaut and Gierlowski-Kordesch, 2010). We interpret the thin, normally graded, and ripple-laminated beds of fine-grained sandstone as products of density flows related to lacustrine underflows or turbidity currents associated with flood conditions and/or spring runoff (e.g., Sturm and Matter, 1978). The disruption of laminations due to fluid escape structures suggests an abundance of pore water within the interstices of the mud, and we interpret that these structures formed as a result of dewatering related to rapid deposition. In general, we interpret that deposition of facies 3 likely occurred in widespread shallow lacustrine

environments with episodic deposition of fine-grained sands delivered from surrounding low-gradient streams during flood conditions.

Facies 4. Tephra beds.

Description: Volcanic ash deposits are common in the lower member and have an average bed thickness of 1 m, with a range in bed thicknesses from 4 cm to 5 m (Figs. 7, 8B, and 8E). These strata are laterally continuous at the scale of the exposures and contain abundant vesicular volcanic glass shards and euhedral phenocrysts (Fig. 8F). Tephra beds commonly have sharp basal contacts and contain laminations that normally grade into finegrained, organic-rich layers at the tops of the beds (Fig. 8E). This facies makes up 4% of the lower member and is best exposed in measured sections 4, 5, and 6 in Figure 7.

Interpretation: We interpret facies 4 to represent air-fall tephra deposited in mainly lacustrine environments represented by facies 3. The absence of flattening/welded fabrics, the laterally continuous bed geometries, the sharp lower contacts, and the gradational upper contacts are common characteristics of air-fall tephras deposited during volcanic eruptions (Smith, 1991). The preservation of laminations and the euhedral phenocrysts within this facies both suggest a lack of extensive reworking by fluvial processes and are consistent with deposition in lacustrine and paludal environments (e.g., Smith, 1991).

Facies 5. Lignite with thin tephra layers.

Description: Lignite beds are common throughout the lower member and often contain thin, laminated tephra layers (Fig. 8E). The average bed thickness of this facies is 20 cm, with a maximum thickness of 50 cm. This facies makes up 2% of the lower member and is best exposed at measured sections 4, 5, and 6 in Figure 7.

Interpretation: We interpret facies 5 to represent deposition in environments with high preservation potential such as swamps, marshes, and other wet floodplain areas (e.g., McCabe, 1985). In our interpretation, these peat-forming environments were inundated by frequent volcanic air-fall events to preserve the thin tephra beds during the deposition of facies 5.

#### Summary of Depositional Systems of the Lower Member

We interpret the abrupt changes in facies types, the documentation of mainly traction-dominated streamflow sedimentary structures, and the common occurrence of woody debris and lignite as products of deposition in stream-dominated alluvial-fan systems (e.g., Ridgway and DeCelles, 1993; Jo et al., 1997; Ghinassi and lelpi, 2016). In contrast to better-studied "arid" alluvial-fan deposystems, these types of alluvial fans are dominated by streamflow facies and are sometimes referred to as wet fans (e.g., Schumm et al., 1987). In our interpretation of the lower member of the McCallum formation, stream-dominated alluvial fans transported sediment into more distal extensive lacustrine environments (Fig. 9). The granule to pebble conglomerate interbedded with coarse sandstone of facies 1 is interpreted to represent deposition in the proximal parts of stream-dominated alluvial-fan

systems adjacent to the major faults along the northeastern basin margin (Fig. 9). Basinward, the proximal facies grade into horizontally stratified, medium-grained sandstone (facies 2) that contains lenses of granule to pebble conglomerate (Fig. 9). Locally, within these facies, there are chaotic mixtures of large, fossilized plant fragments, suggesting that, at times, channels in the stream-dominated alluvial-fan systems were choked with woody detritus, probably during larger flood events. Common distal lithofacies include laminated mudstone (facies 3), tephra (facies 4), and lignite (facies 5). These distal facies are interpreted to represent shallow lacustrine and wetland depositional environments (Fig. 9). Tephras (facies 4) are interpreted to represent widespread air-fall events likely related to volcanic activity of late Miocene volcanic centers of the Wrangell arc (Fig. 9; i.e., Mount Blackburn volcanic center). Published K-Ar dates from these volcanic centers range in age from 6 to 5 Ma (Richter et al., 1990), which overlap the range of 40 Ar/39 Ar dates for the tephras documented in our study for the lower member (6.1-4.9 Ma). The common occurrence of thin tephra horizons in lignite beds suggests that volcanism was nearly continuous at geologic time scales during deposition of the lower member. The common occurrence of lignitic beds along with the abundance of woody and plant detritus in all lithofacies indicates that the landscape was vegetated during deposition of the lower member. We interpret the lower member of the McCallum formation to represent a late Miocene period of basin subsidence, when subsidence outpaced both development of well-integrated fluvial systems and sediment supply, resulting in the development of a regional lacustrine system with adjacent peat swamps (Fig. 9; e.g., McCabe, 1985; Ridgway et al., 2007b).

#### Stratigraphic Context of the Upper Member

The upper member of the McCallum formation is defined mainly by pebble-cobble conglomerate interbedded with coarse-grained sandstone and minor tephra, and it has a minimum thickness of 383 m (Fig. 6A). Two of the lithofacies documented in the lower member are also found in the upper member. These are fine-grained sandstone with siltstone and lignite of facies 3 that constitutes 7% of the upper member, and tephra beds of facies 4 that make up <1% of the upper member (Table 1). In the upper member, facies 3 has an average bed thickness of 4.5 m, contains well-preserved fossil leaves, and is best exposed in measured section 11 in Figure 10. Facies 4 in the upper member has an average bed thickness of 15 cm with a range from 5 to 30 cm and is best exposed in measured section 7 in Figure 10. Tephras in the upper member are thinner (<30 cm) and less common relative to the lower member. The stratigraphically lowest dated tephra in the upper member has a 40Ar/39Ar age of  $5.05 \pm 0.10$  Ma (measured section 7 in Fig. 10), and the stratigraphically highest dated tephra in this member has an age of 3.80 ± 0.05 Ma (measured section 10 in Fig. 10). The most accessible and well-exposed parts of the upper member are along McCallum Creek, and we informally define this exposure as the type section (measured section 9 in Fig. 2; see also Fig. 10).

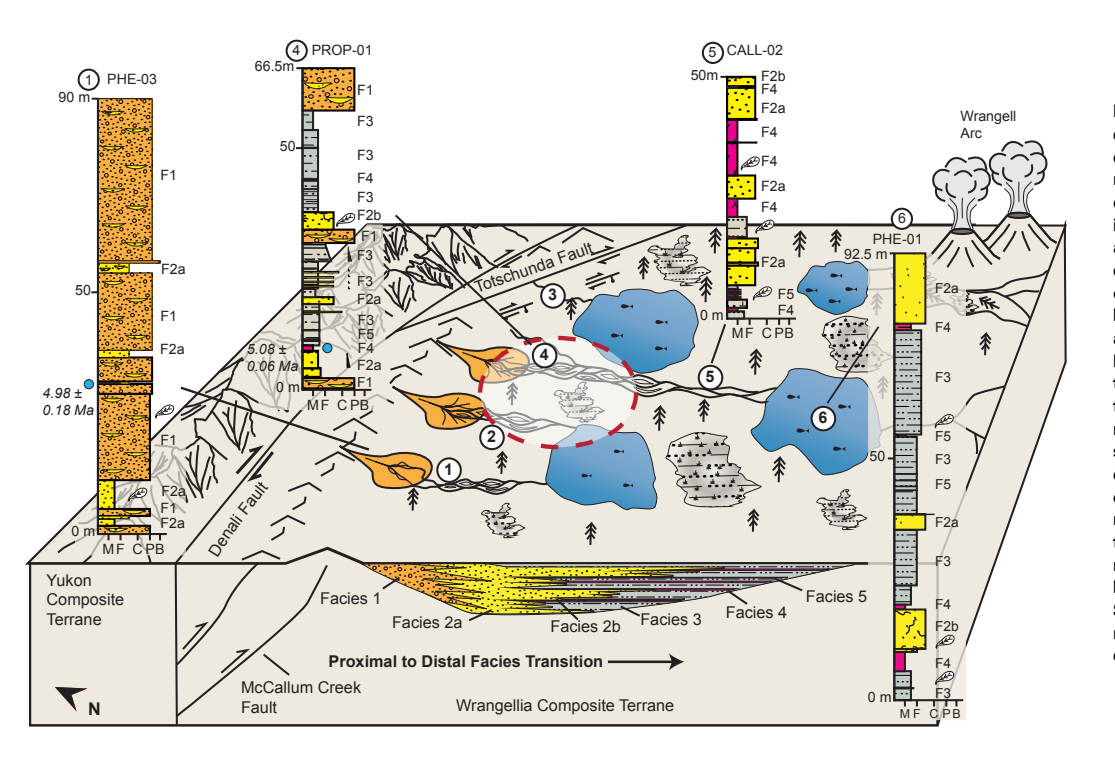


Figure 9. Schematic paleogeographic block diagram of the McCallum basin during late Miocene to early Pliocene deposition of the lower member (ca. 6.17 to ca. 5.0 Ma). Localized, vegetated alluvial fans prograded southwestward into lacustrine-dominated settings. Tephras are best preserved in the more basinward lacustrine deposits. Note the red dashed outline of the approximate position of the McCallum basin near the intersection of the Totschunda and Denali fault system based on Pleistocene-Holocene slip rates along the Kimball section of the Denali fault (13 mm/yr), and the oldest dated tephra of the lower member (ca. 6.17 Ma). Also, note interpreted relative locations of measured sections (circled numbers) in this proximal to distal depositional context and respective facies. Measured sections are intended to show representative lithofacies for different parts of the interpreted depositional setting and do not represent specific time slices for the McCallum basin. See Figure 6 for grain-size abbreviations. See key in Figure 7 for lithofacies patterns in the measured section, and see text and Table 1 for a detailed description of the facies.

## Common Lithofacies of the Upper Member

**Facies 6.** Clast-supported, boulder-pebble conglomerate with minor sandstone.

Description: Facies 6 consists of upward-fining packages of moderately sorted, clast-supported, boulder-pebble conglomerate, and sandstone that range in thickness from 6 to 15 m (Fig. 11A). The lower parts of these packages contain conglomerate beds with crude horizontal stratification. The upper parts of the packages consist of coarse-grained, massive sandstone beds with lenses of conglomerate (Fig. 11A). The contact between the lower conglomerate beds and upper sandstone beds is very gradational. The conglomerate beds exhibit normal grading and contain subrounded to angular clasts with an average maximum particle size of 16 cm and range from 8 to 32 cm (Fig. 11B). Locally, clasts in the conglomerate beds are imbricated. The dominant clast type for all the conglomerate lithofacies of the upper member is metabasalt (greenstone) (Fig. 6B). Within conglomerate packages, there are coarse-grained, lenticular sandstone lenses that have average thicknesses of 3-5 m and widths of 40-50 m. Individual sandstone lenses fine upward in grain size. Within the sandstone lenses, there are thin beds of tephra (facies 4) with thicknesses of 5-30 cm (Fig. 11B). Facies 6 makes up 20% of the upper member and is best exposed at measured section 7 in Figure 10. Facies 6 is only found adjacent to the McCallum Creek thrust fault along the northeastern margin of the McCallum basin (measured section 7 in Fig. 2). Our mapping shows that the boulder conglomerate of facies 6 transitions to finer-grained conglomerate of facies 7 over ~1.5 km (Fig. 2).

Interpretation: We interpret facies 6 to represent proximal facies within a stream-dominated, alluvial-fan system. High-velocity, streamflow processes entrained, transported, and deposited clast-supported, boulder to pebble conglomerate of facies 6 under tractional conditions. The clast-supported texture, crude horizontal stratification, and locally imbricated clasts require that streamflow velocities would have been sufficient to allow bedload transport of coarse clasts (e.g., Rust and Jones, 1987; Collinson, 1996; Miall, 2010). We interpret the sandstone beds that overlie the conglomerate beds as representing lower-flow-velocity deposition during waning flow conditions and/or after the main channel had avulsed to a different part of the channel complex. Our alluvial-fan interpretation is partly based on the restriction of this facies to the immediate footwall of the McCallum Creek thrust fault and the abrupt transition to facies 7.

Facies 7. Organized, clast-supported, pebble-cobble conglomerate with sandstone.

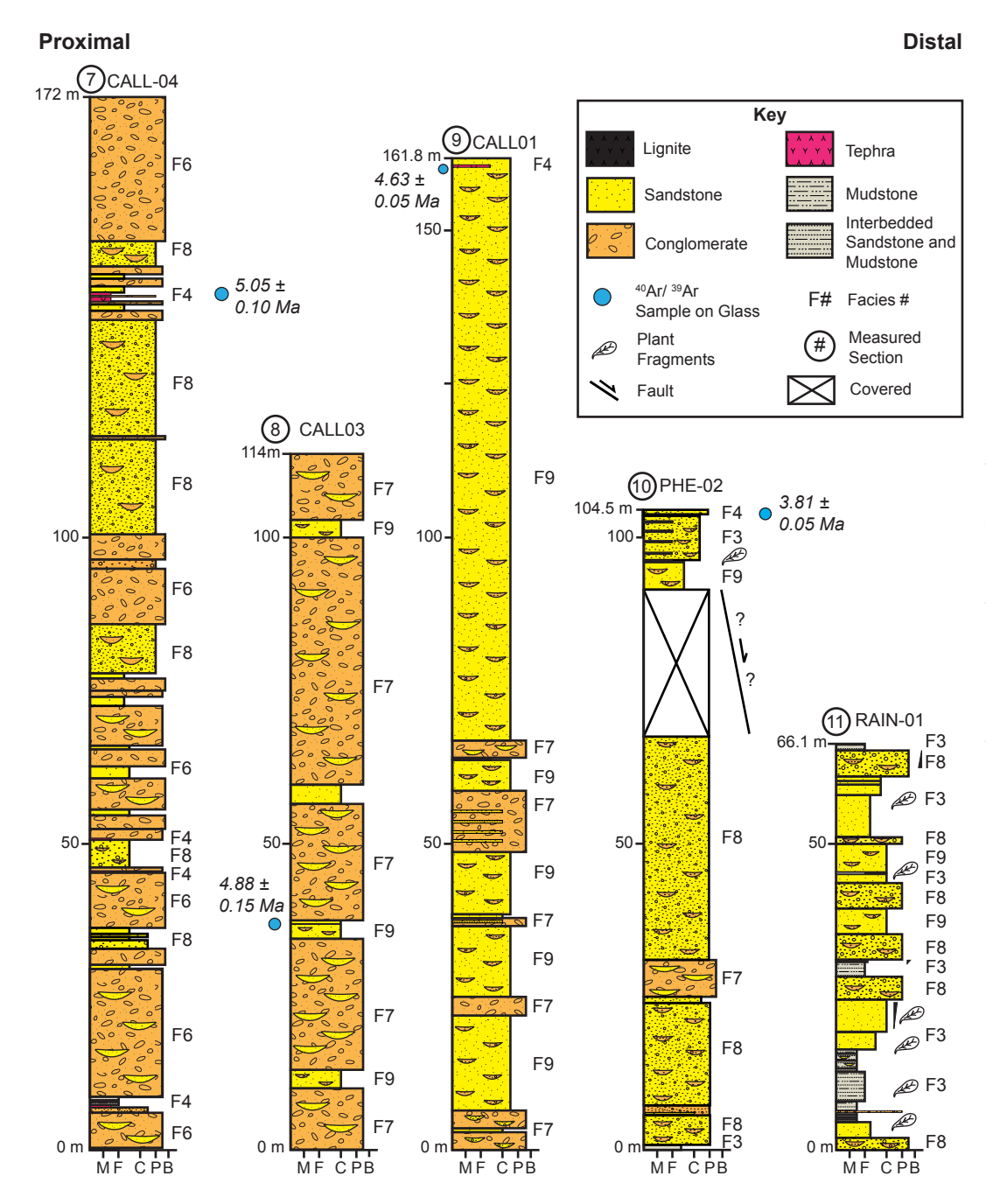
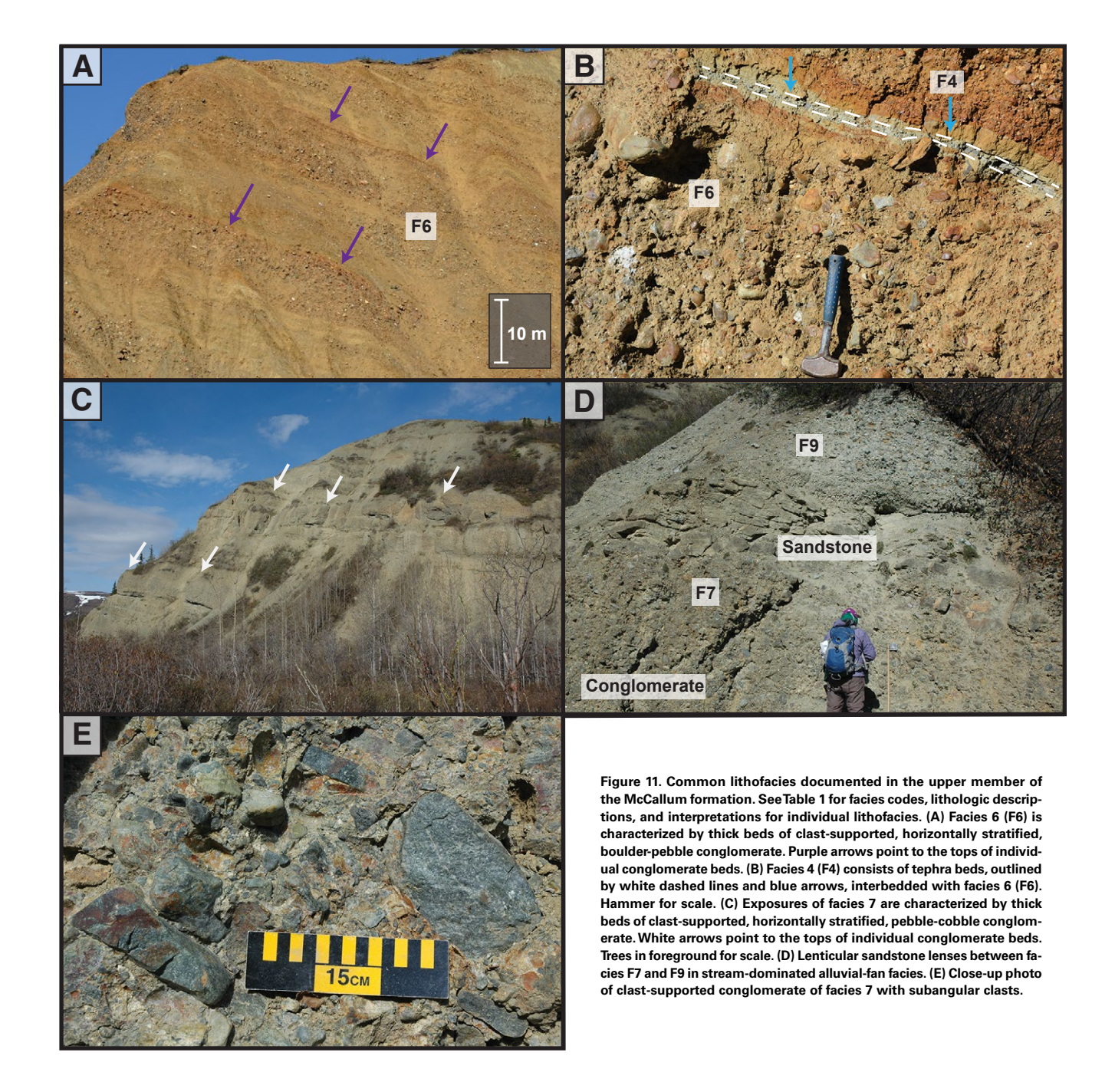


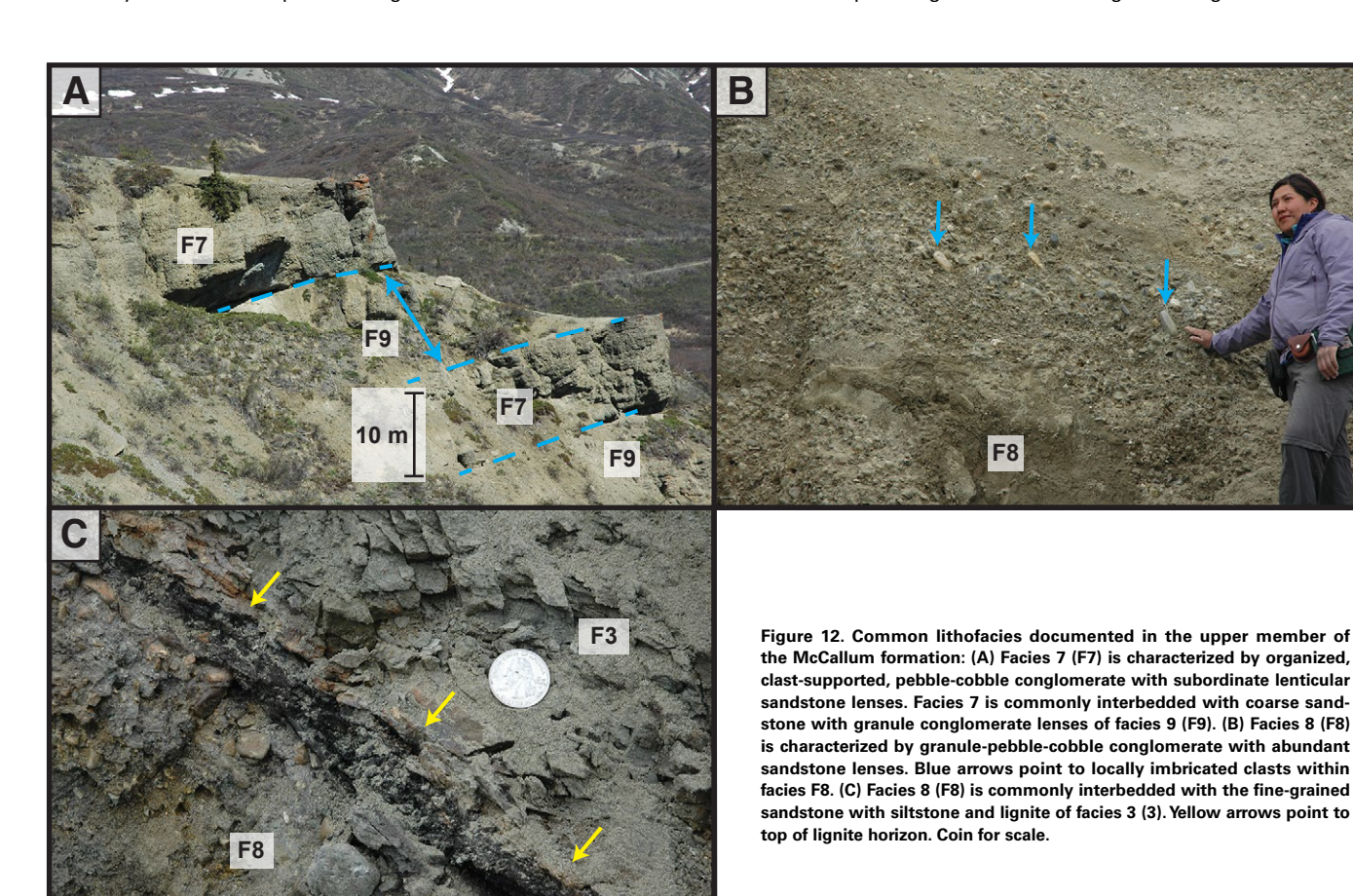
Figure 10. Individual detailed measured sections from the upper member of the McCallum formation showing lithologies, facies distribution, and stratigraphic positions of tephras dated with 40Ar/39Ar geochronology. Each measured section number correlates with their respective geographic locations in Figure 2. Each facies number correlates with their respective detailed facies description discussed in the text and summarized in Table 1. The relative position of each measured section in this figure represents an interpreted proximal to distal basinal location as discussed in the text. Both measured sections and facies numbers also correlate with their location in the interpreted depositional setting for the upper member shown in Figure 13. See Figure 6 for explanation of grain-size abbreviations.



Description: Facies 7 consists mainly of packages of conglomerate interbedded with sandstone and has thicknesses that range from 4.5 to 14 m (Fig. 11C). Conglomerate beds consist of clast-supported, pebble-cobble conglomerate with subordinate lenticular sandstone lenses (Fig. 11D). These conglomerate packages are dominated by horizontal stratification in broad 50–60-m-wide lenticular units that are 10–12 m thick (Fig. 11C). The conglomerate beds commonly contain imbricated, subrounded to rounded clasts that have an average maximum particle size of 9 cm and range in size from 5 to 16 cm (Fig. 11E). Sandstone units within the conglomerate consist of discontinuous, coarse- to medium-grained sandstone lenses with lenticular geometries with a range of thicknesses from 10 to 20 cm. The upper contacts of these conglomerate units are commonly overlain with upward-fining sandstone beds that consist of

coarse- to medium-grained, horizontally stratified sandstone with bed thicknesses that range from 0.50 to 1 m (Figs. 11D and 12A). Facies 7 makes up 31% of the upper member and is best exposed in measured sections 8 and 9 in Figure 10. This facies grades northeastward into coarser-grained conglomerate of facies 6 and southwestward into finer-grained conglomerate of facies 9.

Interpretation: We interpret the clast-supported conglomerate with horizontal stratification and lenses of lenticular sandstone of facies 7 as being indicative of deposition by streamflow processes. These are characteristics of gravels transported as bedload by tractive currents under hydrodynamically stable flow conditions to form longitudinal bars (e.g., Collinson, 1996; Lunt and Bridge, 2004; Nichols and Fisher, 2007). Imbrication is best developed across the top of longitudinal bars in high-discharge areas of streamflow



(Collinson, 1996). Reduction in flow velocities allows for sand to be deposited through rapid saltation or suspension processes on the tops of gravel-rich bars (Collinson, 1996). We interpret these conglomerate units as representing deposition in shallow braided channels in the medial region of a stream-dominated alluvial-fan system.

**Facies 8.** Well-organized, sandy, clast-supported, granule-pebble-cobble conglomerate with sandstone.

Description: Facies 8 consists of conglomerate beds interbedded with sand-stone that range in thickness from 1 to 10 m and amalgamate to thicknesses up to 19 m based on our measured sections. Conglomerate units consist of well-sorted, imbricated, clast-supported, granule-pebble-cobble conglomerate with abundant sandstone lenses (Fig. 12B). Clasts in the conglomerate are commonly subrounded and have an average maximum particle size of 6 cm with a range in size from 4.5 to 14 cm (Fig. 12C). Sandstone lenses within the conglomerate consist of coarse-grained sandstone beds that range in thickness from 5 to 20 cm and often contain trough cross-stratification. These sandstone lenses are discontinuous at width scales of 5–6 m. This facies makes up 20% of the upper member and is best exposed in measured sections 7, 10, and 11 in Figure 10. Facies 8 grades east-northeastward into coarser-grained conglomerate of facies 7 and west-northwestward into the sandstone-dominated facies 9 and facies 3.

Interpretation: We interpret the clast-supported conglomerate with imbricated clasts and trough cross-stratification of facies 8 to indicate deposition by streamflow processes. The grain size of clasts, thickness of conglomerate beds, and high sandstone content in this facies are interpreted to represent distal parts of stream-dominated alluvial-fan systems (e.g., Ghinassi and lelpi, 2016).

**Facies 9.** Sandstone with abundant granule conglomerate lenses.

Description: Facies 9 consist of horizontally stratified, coarse-grained sandstone units containing conglomeratic lenses (Fig. 11D). Bed thicknesses of these sandstone units range from 3 to 10 m (Fig. 12A) and have amalgamated thicknesses as much as 84 m. Sandstone units commonly contain granule conglomerate lenses, but, locally, pebble conglomerate lenses have an average maximum particle size of 4 cm with a range in size from 3 to 7 cm. Horizontal stratification is very common in this facies. This facies makes up 8% of the upper member based on our measured sections and is best exposed in measured section 9 in Figure 10.

Interpretation: We interpret the horizontally stratified, thick-bedded sand-stone with lenticular granule conglomerate lenses as representing deposition in sandy bedload channels (e.g., Collinson, 1996; Nichols and Fisher, 2007; Fisher et al., 2007; Miall, 2010). In these types of depositional systems, sand is deposited mainly on midchannel bars, with gravel lenses deposited as basal lags (Fisher et al., 2007). Subordinate conglomerate deposits in facies 9 suggest that average streamflow velocities were insufficient to mobilize coarse gravel detritus and favored transport of finer sand-sized sediment. In our interpretation, this sandstone-dominated facies represents channel deposits located in the medial-distal region of a stream-dominated, alluvial-fan system.

#### Summary of Depositional Systems of the Upper Member

We interpret the upper member to represent a Pliocene period of general basinward progradation of coarse-grained, stream-dominated alluvial-fan deposystems over finer-grained, lacustrine-dominated deposystems of the lower member (Fig. 13). Boulder-pebble conglomerate of facies 6, located directly in the footwall of the McCallum Creek thrust fault, is interpreted as proximal stream-dominated alluvial-fan strata (Fig. 13). These strata grade basinward into better-organized cobble-pebble conglomerate of facies 7, which we interpret as medial alluvial-fan strata (Fig. 13). These deposits grade basinward into granule-pebble conglomerate of facies 8 and sheet sandstone of facies 9, which we interpret as the more distal parts of stream-dominated alluvial-fan depositional systems (Fig. 13). The fine-grained sandstone interbedded with siltstone and lignite of facies 3 in the upper member contains well-preserved fossil leaves and is only present in our most distal measured section (measured section 11 in Fig. 10). These lithologies are interpreted as having been deposited in lacustrine, wetland, and other vegetated paludal environments, and they are interpreted as the most distal lithofacies studied in the upper member (Fig. 13).

The south-southwestward paleoflow indicators for the upper member (Fig. 6A), which collectively have a general radial pattern, are consistent with an alluvial-fan interpretation. We interpret the predominance of metabasalt (greenstone) clasts in the conglomerate of the upper member (Fig. 6B) as an indication that the stream-dominated alluvial fans were transporting sediment derived from the metabasalt-rich Slana Spur Formation and Nikolai Greenstone exposed in thrust sheets that define the northeastern margin of the McCallum basin (Fig. 2). These stratigraphic and structural relationships are discussed in the next section. Our 40Ar/39Ar tephra dates from the upper member (5.0–3.8 Ma) overlap well with the published K-Ar dates near Mount Blackburn (4.5–3.4 Ma), a Pliocene volcanic center of the Wrangell arc (Richter et al., 1990).

## Structural and Stratigraphic Relationships along the Eastern Basin Margin

The northwest-to-southeast-trending McCallum Creek thrust system defines the northeastern margin of the McCallum basin and is a key area in which to examine structural and stratigraphic relationships (Fig. 14A). In most places, the McCallum Creek fault places Pennsylvanian-Permian igneous rocks in the hanging wall of the thrust fault over Upper Miocene-Pliocene McCallum formation in the footwall (Figs. 14B and 14C). In Figure 14B, proximal strata of the upper member of the McCallum formation (facies 6) in the footwall dip ~30°N toward the fault contact (measured section 7 in Fig. 2; Fig. 11A). Southeastward, the McCallum Creek fault juxtaposes Eocene volcanic and volcaniclastic strata over Upper Miocene strata of the lower member of the McCallum formation (Gillis et al., 2019). Here, footwall strata are dipping 45°

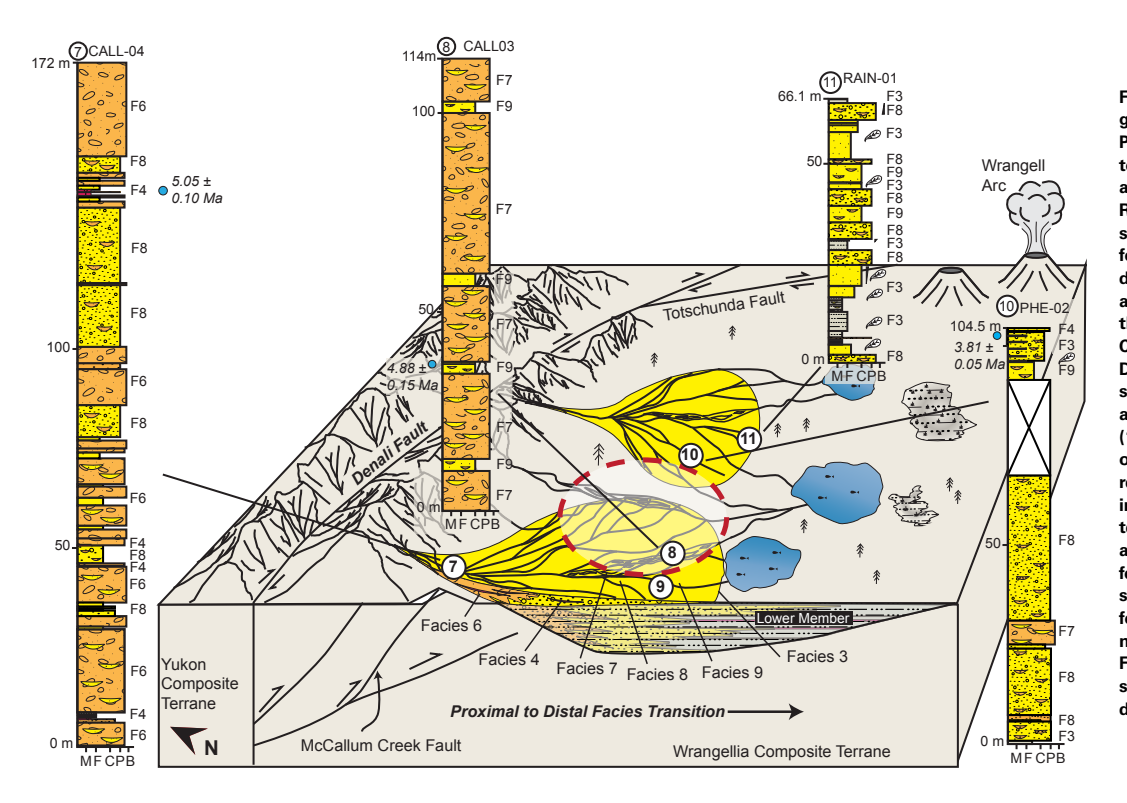


Figure 13. Schematic paleogeographic block diagram of the McCallum basin during early to late Pliocene deposition of the upper member (5.0 Ma to 3.8 Ma). Coarse-grained, stream-dominated alluvial fans prograded over the lower member. Rapid subsidence driven by flexural loading of southward-propagating thrust sheets allowed for the continued preservation of volcanic ash deposits during eruptive periods of the Wrangell arc. Note the red dashed outline that indicates the approximate tectonic position of the Mc-Callum basin in a transpressional section of the Denali fault system. Tectonic transport of the basin is based on Pleistocene-Holocene slip rates along the Kimball section of the Denali fault (13 mm/yr) and the age of the oldest tephra of the upper member (ca. 5.0 Ma). Also note relative locations of measured sections in this interpreted proximal to distal depositional context and respective facies. Measured sections are intended to show representative lithofacies for different parts of the interpreted depositional setting and do not represent specific time slices for the McCallum basin. See Figure 6 for explanation of grain-size abbreviations. See key in Figure 7 for lithofacies patterns of the measured sections, and see text and Table 1 for a detailed description of the facies.

toward the fault (Figs. 14D and 14E; measured section 3 in Fig. 2). Along this part of the fault trace, zircon U-Pb geochronology (utilizing multigrain laserablation-inductively coupled plasma-mass spectrometry) on Eocene volcanic strata in the hanging wall yielded an age of 50 Ma (Fig. 14E, location 1; Table S2 [footnote 1]), whereas a tephra in the McCallum formation, located in the footwall, has a 40Ar/39Ar date of 6.17 ± 0.07 Ma (Fig. 14E, location 2). In Figure 14F, a steeply dipping tephra bed of the lower member is shown that has a  $^{40}$ Ar/ $^{39}$ Ar date of 5.1  $\pm$  0.06 Ma. Generally, we observe that strata of the McCallum formation in the footwall have been steeply tilted with dips from 30° to 80° near the contact with the McCallum Creek thrust fault. Our field observations as shown in Figure 14 and recent work by Waldien et al. (2018) are consistent with the upper member of the McCallum formation being deposited in a transpressional basin related to a westward (basinward) propagating thrust system. Geologic mapping and structural data indicate that this thrust system is part of a regional flower structure that soles into the strike-slip Denali fault system, which is located ~10 km northeast of the study area (Fig. 2; Waldien et al., 2018). These observations are all evidence of Neogene deformation along this part of the Denali fault system, and they are consistent with documentation of multiple aftershocks of the 2002 Denali earthquake that were located on the McCallum Creek fault (e.g., Brocher et al., 2004). The seismicity augments geomorphic data that indicate the McCallum Creek thrust system is an active component of the Denali fault system (Waldien, 2015) and that related basin development continues to the present.

### DISCUSSION

#### Stages of Neogene Basin Development and Strike-Slip Displacement

Establishment of a depositional, chronostratigraphic, and structural framework for the McCallum formation provides an opportunity to evaluate Neogene basin development and strike-slip displacement along the Denali fault system. Figure 15A illustrates the following: the modern tectonic configuration of the McCallum basin relative to the Denali and Totschunda faults, the surface rupture

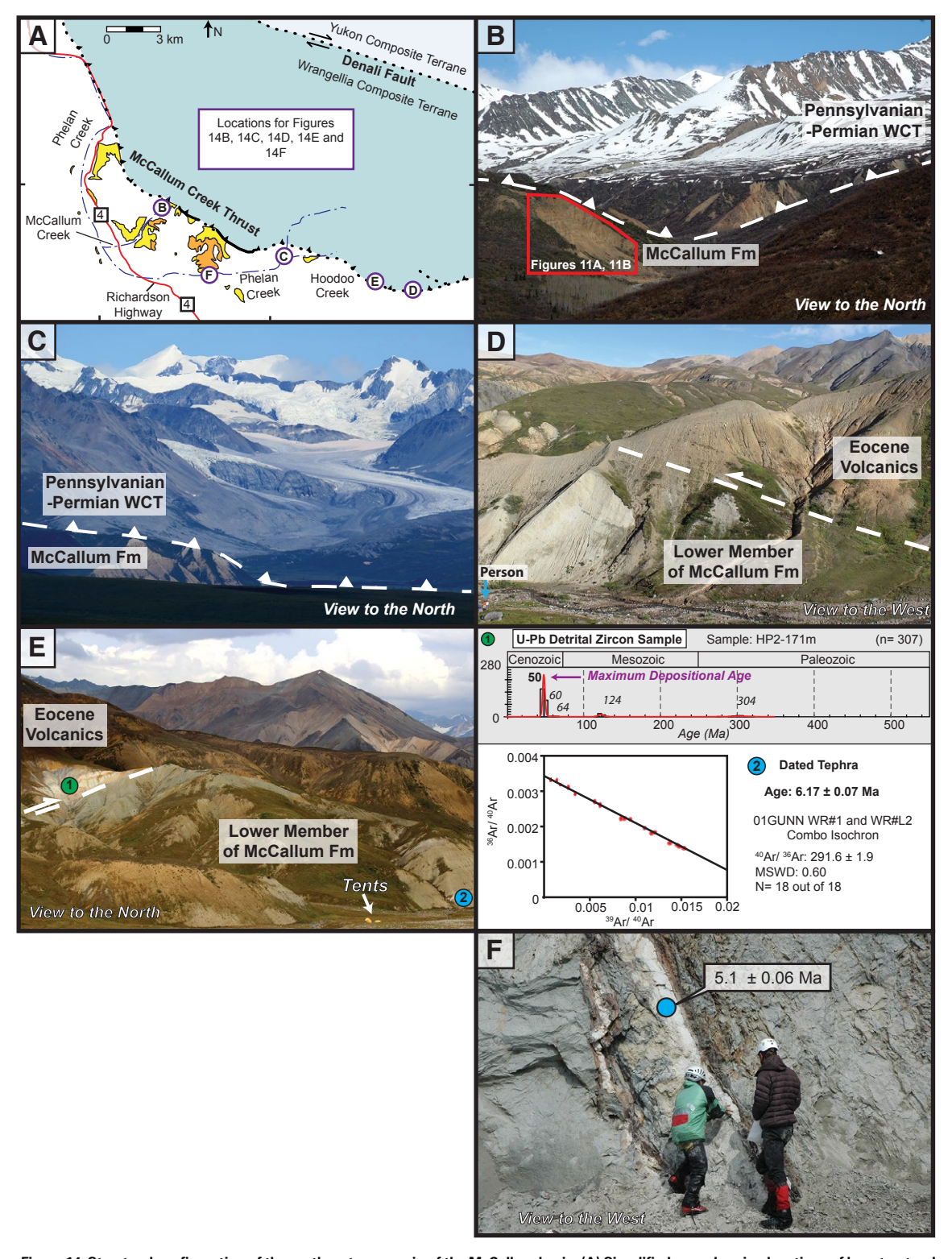
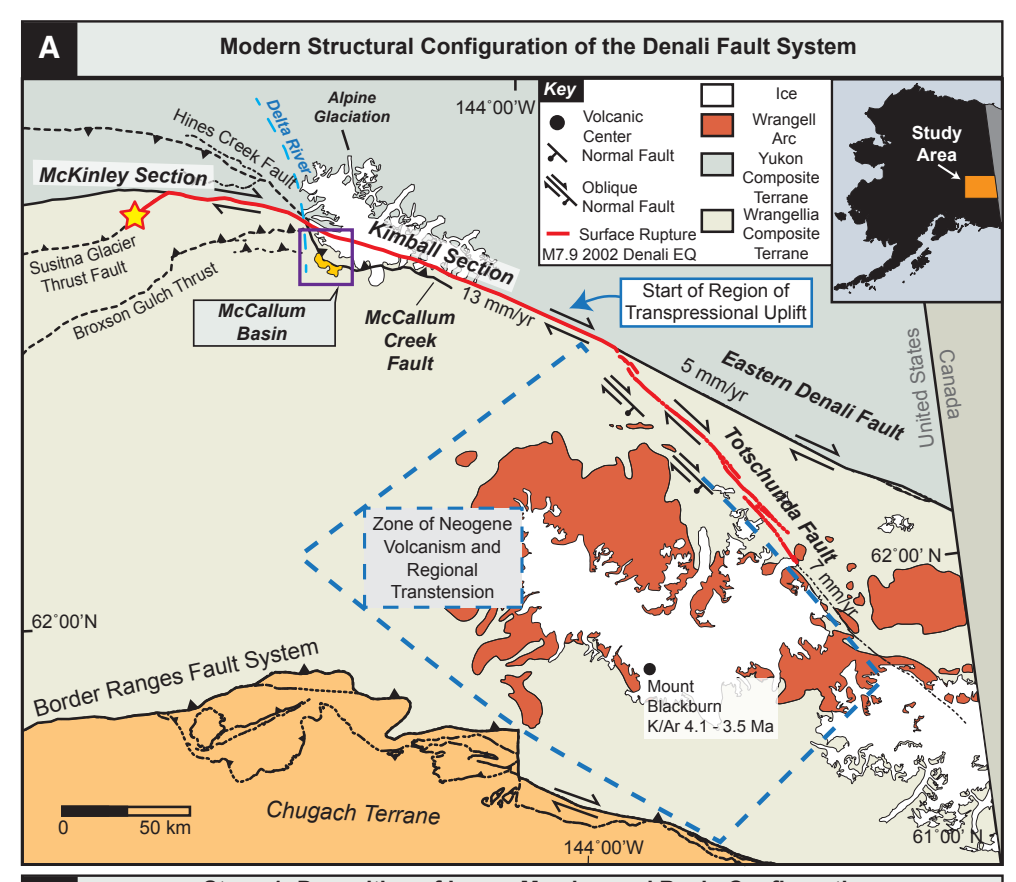


Figure 14. Structural configuration of the northeastern margin of the McCallum basin: (A) Simplified map showing locations of key structural and stratigraphic relationships documented between the McCallum Creek fault and the McCallum formation. Circled locations B through F on map correspond with photographs shown in parts B–F. (B–C) Pennsylvanian–Permian rocks of the Wrangellia composite terrane (WCT) in hanging wall juxtaposed with proximal alluvial-fan strata of the upper member of the McCallum formation in the footwall. (D–E, left column) Eocene volcanic rocks in the hanging wall juxtaposed with lower member of the McCallum formation in the footwall. White dashed line in both photos represents location of thrust fault. Blue arrow in D points to person (red shirt) and white arrow in E points to yellow tents for scale. (E, right column) Age determination plots from circled locations shown in adjacent photo, showing 50 Ma U-Pb zircon age for Eocene volcanic ash deposit at location 1 in the hanging wall (white bed; Table S2 [text footnote 1]) and <sup>40</sup>Ar/<sup>39</sup>Ar date of tephra of 6.17 Ma at location 2 in the footwall (measured section 3 in Fig. 7). MSWD—mean square of weighted deviates; WR—whole-rock sample. (F) Steeply dipping tephra (white bed) with the determined <sup>40</sup>Ar/<sup>33</sup>Ar date of 5.1 Ma in the lower member of the McCallum formation (from measured section 4 in Fig. 7).



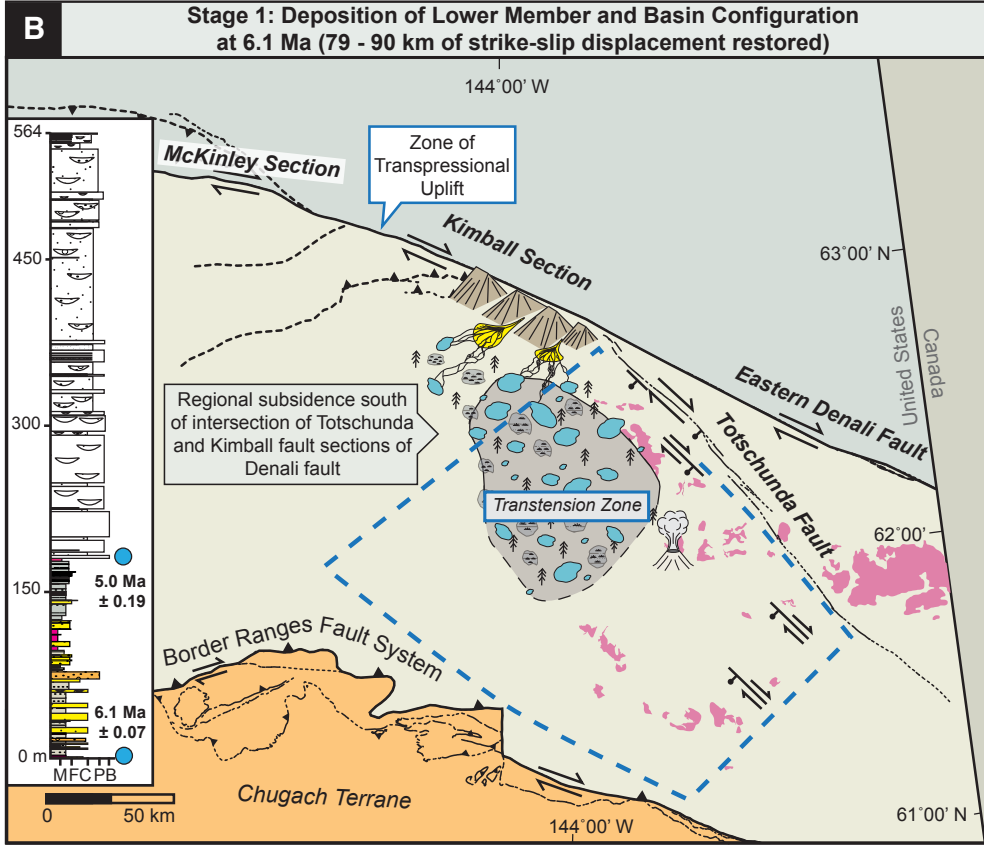
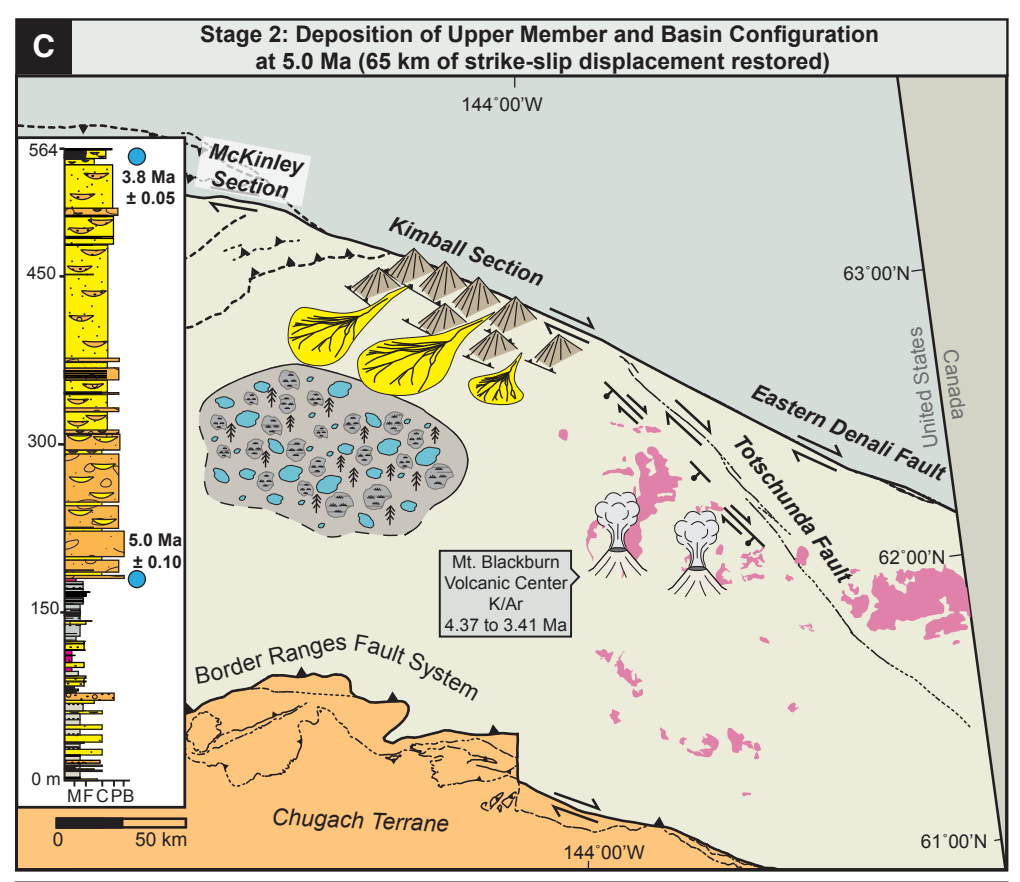


Figure 15. Schematic depositional and strike-slip displacement models that illustrate the interpreted stages of McCallum basin development based on chronostratigraphic and modern slip rates along the Denali fault system. (A) Modern structural configuration of the Denali fault system highlights a region of Neogene transtension and volcanism between the Totschunda and Border Ranges fault systems. The junction of the Totschunda and Denali faults marks the start of a zone of transpressional uplift. Farther northwest of this junction, deformation is characterized by thrust deformation north and south of the Denali fault as rock is transported into an area of increasing transpression along the more westward-trending Kimball and McKinley sections of the fault system. The epicenter (yellow star) and the 341 km surface rupture of the M 7.9 Denali earthquake (EQ) is outlined by the red line (from Haeussler, 2009) to highlight active strike-slip active tectonics along the Denali fault system in the study area. (B) Stage 1: 6.1-5 Ma. During regional lacustrine deposition of the lower member, the McCallum basin is interpreted to have been located ~79 km to the southeast of its current location based on Pleistocene-Holocene slip rates (13 mm/yr). Active volcanism resulted in preservation of numerous and thick tephras throughout the lower member. (Continued on following page.)



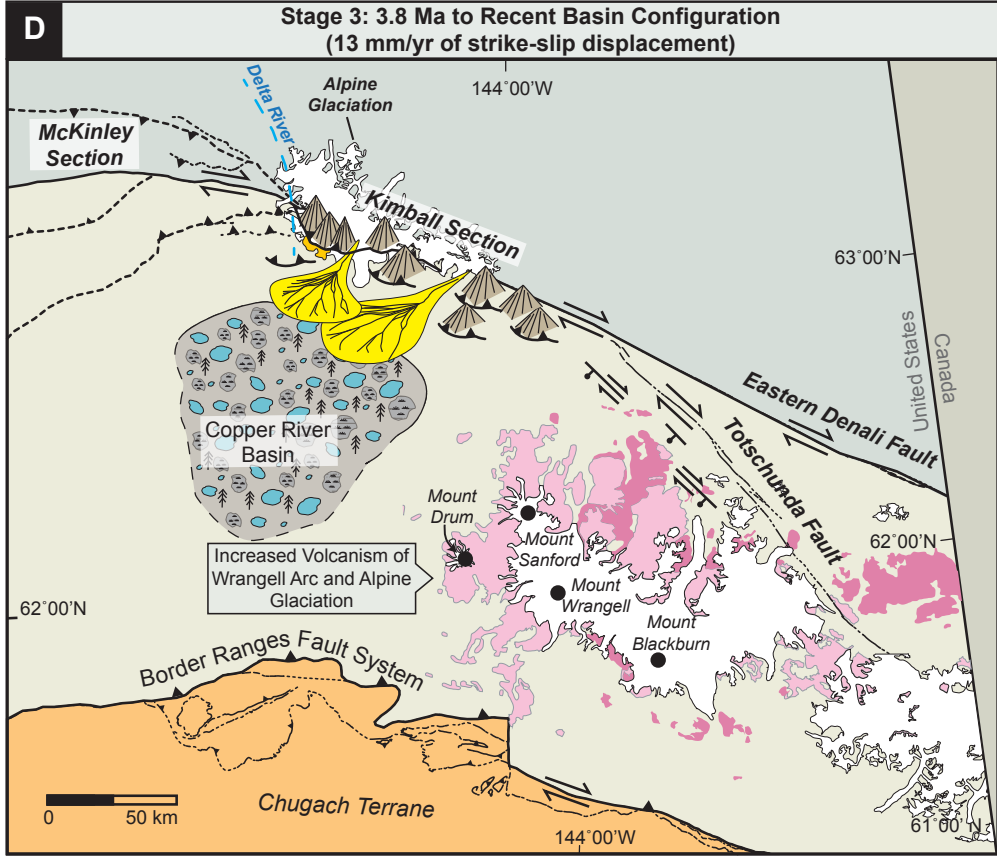


Figure 15 (*Continued*). (C) Stage 2: 5.0-3.8 Ma. During strike-slip transport of the McCallum basin along the Kimball section, rocks of the Wrangellia composite terrane, exposed in the hanging wall of the McCallum Creek fault, were exhumed and supplied sediment to extensive alluvial-fan and braided stream systems in the basin. These coarse-grained depositional systems prograded over the finer-grained lacustrine deposits of the lower member. The McCallum basin is interpreted to have been located ~65 km southeast of its present position at the start of this stage. Dates for volcanism near Mount Blackburn are from Richter et al. (1990). (D) Stage 3: 3.8 Ma to recent. Depositional setting: The proximal parts of the McCallum basin are being deformed and exhumed. These reconstructions are based on Pleistocene-Holocene slip rates from Haeussler et al. (2017a). Modern structural configuration and Wrangell arc geologic units are derived from Wilson et al. (2015) and Trop et al. (2012). See Figure 6 for stratigraphic section legend and explanation of grain-size abbreviations.

of the M 7.9 2002 Denali earthquake, a series of south-verging thrust faults along the south side of the Denali fault, and the Wrangell arc. We interpret several distinct stages of basin development since ca. 6.1 Ma based on our stratigraphic and geochronologic analyses of the McCallum formation; each of these progressive stages is shown in Figures 15B-15D. These stages are interpreted to record the northwestward strike-slip transport of the McCallum basin from a zone of transtensional deformation that starts near the junction of the Totschunda and Denali faults, as shown in Figure 15A, into a region of partitioned transpressional deformation characterized by shortening along the south side of the Denali fault northwest of the junction of the Totschunda and Denali faults. Geologically, the transtensional section is characterized by the following: ~2 mm of active extension on the dextral strike-slipTotschunda fault, based on geodetic data (Elliott and Freymueller, 2020), Neogene normal faults (Trop et al., 2012), and Neogene volcanism (Richter et al., 1990; Preece and Hart, 2004; Berkelhammer et al., 2019; Brueseke et al., 2019; Trop et al., 2022). The transpressional section is characterized by a strike-slip flower structure and south-verging thrust faults that include the McCallum Creek thrust system on the dextral Denali fault (e.g., Ridgway et al., 2002; Riccio et al., 2014; Waldien et al., 2018). Farther to the west, thrust systems and related sedimentary basins are present on both the north and south sides of the Denali fault system (Fig. 15A; Ridgway et al., 2002, 2007b; Bemis and Wallace, 2007; Lesh and Ridgway, 2007; Bemis et al., 2012, 2015; Riccio et al., 2014; Burkett et al., 2016; Haeussler et al., 2017b). One of these thrust faults, the south-verging Susitna Glacier thrust fault (Fig. 15A), was the epicenter for the 2002 Denali earthquake. This earthquake propagated from the thrust fault onto the Denali fault and then migrated southward onto the Totschunda fault (Fig. 15A; Eberhart-Phillips et al., 2003; Crone et al., 2004; Haeussler et al., 2004). As discussed in the following sections, our preferred interpretation for the northward strike-slip transport of the McCallum basin along the Denali fault system is similar to the general trace of the 2002 Denali earthquake surface rupture.

## Stage 1 (6.1–5.0 Ma): Transtensional Basin Development and Lacustrine-Dominated Depositional Systems (Fig. 15B)

From a strike-slip displacement perspective, we repositioned the basin during stage 1 to accommodate an interpreted displacement of ~79–90 km of dextral offset of the McCallum basin since ca. 6.1 Ma, as shown in the paleogeographic reconstruction in Figure 15B. In this reconstruction, the McCallum basin would have been located near or adjacent to the Denali-Totschunda fault junction in an area presently characterized by transtension. Our reconstruction is based on extrapolating Pleistocene–Holocene slip rates on the Kimball (~13 mm/yr) and Totschunda (~7 mm/yr) sections of the Denali fault for 6.1 m.y. (e.g., Matmon et al., 2006; Mériaux et al., 2009; Haeussler et al., 2017a), based on the date of the oldest tephra (6.1 Ma) documented in our study from the McCallum formation. It is important to note that the lower contact of the McCallum formation with underlying "basement" rock has not been identified

in our study area, so our estimates serve as minimum displacement amounts based on the age of the oldest exposed tephra. Using Pleistocene–Holocene slip rates, the McCallum basin would be relocated 79 km southeastward of its current position. Restoration of the McCallum basin fully to the Denali-Totschunda fault junction requires 90 km of displacement. Within this framework, we refer to 79–90 km of strike-slip displacement in the text.

It is important to note that a recent geodetic study has provided present-day slip estimates along the Kimball (6–7 mm/yr), Totschunda (~9–10 mm/yr), and eastern Denali (~2–3 mm/yr) fault sections (Elliott and Freymueller, 2020) that differ from the Pleistocene–Holocene slip rates, with the Kimball section having the largest difference. Our preferred slip estimate for the Kimball section of the Denali fault is based on Pleistocene–Holocene slip estimates, which provide longer records of the slip history, but there is undoubtedly considerable uncertainty for estimating slip rates partitioned along the three fault segments over the last 6.1 m.y. Also note that our approach assumes that the eastern Denali fault has accommodated only minor strike-slip displacement since 6.1 Ma. This assumption may be valid based on a recent seismological study that suggests the eastern Denali fault has been inactive during the past ~6 m.y. (Choi et al., 2021). Our assumption, however, remains an oversimplification in light of reported offset geologic features on the eastern Denali fault near Kluane Lake, Yukon, which suggest ~2 mm/yr of slip (Haeussler et al., 2017a).

From a depositional system perspective, this initial stage of development of the McCallum basin was characterized by extensive lacustrine-dominated environments within the transtensional region near the Denali-Totschunda junction (Fig. 15B). Along the eastern basin margin, localized stream-dominated alluvial-fan systems within vegetated, forest ecosystems (facies 1) transitioned into more medial sand-rich parts of the alluvial-fan complex (facies 2) that merged basinward into more distal widespread shallow lacustrine environments (facies 3). Lateral to the lacustrine environments were well-established, peat-forming wetlands and bogs (facies 5; Figs. 7, 9, and 15B). These distal lacustrine and wetland environments were areas of high preservation potential for the numerous tephras that are common in the lower member and indicate coeval volcanism, likely from the adjacent Wrangell arc (Fig. 15B). This first stage of basin development ended by ca. 5 Ma, based on the 4.98 ± 0.19 Ma date from the youngest dated tephra from the lower member (Figs. 6 and 15B).

## Stage 2 (5.0–3.8 Ma): Transpressional Basin Development and Stream-Dominated Alluvial-Fan Depositional Environments (Fig. 15C)

During the next stage of basin development, we interpret the McCallum basin to have been tectonically transported northwestward of the intersection of the Totschunda and Denali faults into a region of transpressional uplift along the Kimball section of the Denali fault system (Fig. 15C). At the start of stage 2, the basin would have been located ~65 km to the southeast of its current position based on Pleistocene–Holocene displacement rates (~13 mm/yr) and the oldest dated tephra of the upper member (5.0 Ma) (Figs. 6 and 15C).

Transport into this transpressional region is interpreted to be marked by an abrupt change in depositional systems, average grain size, and structural configuration of the basin. This stage was characterized by deposition in conglomeratic stream-dominated alluvial-fan environments that characterize strata of the upper member (Fig. 6). The coarse-grained strata are interpreted to be the product of increased shortening of the thrust system along the northeastern basin margin as the basin was transported farther into the region of transpressional uplift. Continued shortening and exhumation on the interior thrust sheets produced the needed topographic gradient to allow transport of coarser-grained detritus to the McCallum basin. Flexural subsidence produced by the load of the growing thrust system created accommodation space in the basin and resulted in the progradation of more proximal, alluvial fans of the upper member over more distal, lacustrine strata of the lower member (Figs. 6 and 15C).

Apatite fission-track data of Waldien et al. (2018) are consistent with our sedimentologic-based interpretation of the growth of the thrust system along the northeastern margin of the McCallum basin. These data indicate ~4.8 km of exhumation since ca. 6 Ma, based on cooling ages in the hanging wall of the McCallum Creek thrust fault. These young cooling ages suggest that the up-section coarsening in grain size documented for the McCallum formation (Fig. 6) was a product of growth, propagation, and erosion of the thrust system as the basin was transported along the transpressional fault section.

## Stage 3 (3.8 Ma to Present): Active Transpressional Basin (Fig. 15D)

The modern McCallum basin continues to develop as a transpressional basin, with the northeastern margin defined by a southwestward-propagating thrust system (Figs. 2 and 14). The shortening in the thrust system is interpreted to be related to the continued strike-slip transport of the basin along a region of increasing transpressional uplift that transitions westward into the start of the section of the Denali fault sometimes referred to as the Hayes restraining bend (e.g., Fitzgerald et al., 2014; Riccio et al., 2014; Bemis et al., 2015). At the start of stage 3, the basin would have been located ~49 km to the southeast of its current position, based on extrapolation of Pleistocene-Holocene slip rates (~13 mm/yr) since 3.8 Ma (youngest dated tephra). The exposed stratigraphic section appears to continue above the 3.8 Ma tephra but is covered by vegetation in the lowlands. It is also important to note that geophysical studies interpret 1.5 km of subsurface basin fill for the McCallum basin (Morin and Glen, 2003; Brocher et al., 2004), so our 564-m-thick composite section (Fig. 6A) only reflects the part of the stratigraphic section being exposed in the more proximal part of the basin.

In stage 3 of basin development, the northeastern margin of the basin is being overridden by thrust sheets with Pennsylvanian–Permian igneous rocks (Figs. 14B and 14C) and Eocene volcanic strata (Figs. 14D and 14E) in their hanging walls. Locally, proximal parts of the McCallum basin stratigraphy have been incorporated into the basinward thrust sheets. These structural and

stratigraphic relationships result in the northeastern margin of the McCallum basin being locally folded with steeply dipping strata in the proximal footwall (Fig. 14F). Modern and Quaternary deposition in the proximal parts of the McCallum basin is characterized by glacial outwash fan systems that transition into high-gradient, braided fluvial environments that flow into the north-flowing Delta River. Prior to the early Quaternary development of the north-flowing Delta River system (Péwé, 1987), our paleoflow data (Fig. 6A) indicate preglacial, south-southwestward drainages transported sediment toward the region of the modern Copper River basin. Glacial deposits are common in the study area and provide an opportunity for needed future research. The timing of glaciation in the eastern Alaska Range is unclear, but previous studies have estimated 2.9-2.6 Ma for east-central Alaska, 2.5 Ma for the north side of the central Alaska Range, and 3.7 Ma for the western Alaska Range (Denton and Armstrong, 1969; Duk-Rodkin et al., 2004, 2010; Lease et al., 2016). At times during stage 3, the McCallum basin also contained parts of glacial Lake Atna (e.g., Ferrians and Schmoll, 1957; Wiedmer et al., 2010). Volcanic activity continued in this stage of basin development, as marked by three of the largest, by volume, active volcanoes in the Wrangell arc complex (Mount Wrangell, Mount Drum, and Mount Sanford in Fig. 15D; Richter et al., 1990, 1994).

## **Summary of Neogene Strike-Slip Basin Development**

We interpret the stratigraphy and geochronology documented for the McCallum basin to represent a record of sedimentation during transport of the basin from a transtensional to a transpressional setting along the Denali fault system. This transition in the stratigraphic record is characterized by a marked change from predominantly finer-grained lacustrine to coarser-grained alluvial-fan strata (Fig. 6). The transtensional stage of basin formation initiated by ca. 6.1 Ma and ended by ca. 5.0 Ma, based on the dated tephras (Fig. 6). The transpressional stage of basin development started at ca. 5.0 Ma and continues to the present. We interpret this change in depositional systems and basin configuration as a response to the growth, exhumation, and erosion of thrust sheets as the McCallum basin was tectonically transported into a region of transpressional deformation along the Kimball section of the Denali fault system.

Our chronostratigraphic framework for the McCallum basin also provides the opportunity to determine sediment accumulation rates associated with deposition during both transtensional and transpressional stages of basin development. The lacustrine-dominated strata of the exposed portion of the lower member are 181 m thick and were deposited over an ~1 m.y. time span (Fig. 6). The sediment accumulation rate for the deposition of the lower member is ~181 m/m.y. The alluvial-fan strata of the upper member are 383 m thick and were deposited over an ~1.2 m.y. time span (Fig. 6). The sediment accumulation rate for the deposition of the upper member is ~319 m/m.y. These estimates suggest sedimentation rates doubled during the stage of basin development associated with translation into a region of transpressional deformation along

the Denali fault system. It is important to note that these determinations do not account for sediment compaction and that deposition in nonmarine environments is often discontinuous and marked by hiatuses. We realize that these are high sediment accumulation rates, but they are not outside the realm of possibilities, considering that the Pliocene–Pleistocene foreland basin of Taiwan has sedimentation rates up to 1900 m/m.y. (Chen et al., 2001).

The sedimentary record of strike-slip basin development along continental strike-slip fault systems is often difficult to elucidate due to low preservation potential, structural complexity, and multiple unconformities, leading to an incomplete stratigraphic record (e.g., Sylvester and Smith, 1976; Christie-Blick and Biddle, 1985). Prior studies of strike-slip basin development have focused on distinct end members of basin types termed transpressional and transtensional basins (for a comprehensive review of both types of basins, see Mann, 2007). Subsidence mechanisms for each setting vary, with localized extension being a dominant subsidence mechanism for transtensional basins and flexural subsidence being a dominant subsidence mechanism for transpressional basins (Ingersoll, 2011). Our analysis of the McCallum basin defines a composite basin type that initiated in a transfensional setting and was subsequently transported into a transpressional setting (e.g., Reading, 1980). Our findings suggest that the McCallum basin may serve as an example of what we term a "composite" strike-slip basin, characterized by a stratigraphy that records distinct stages of basin development along a major strike-slip fault system. Because continental strike-slip fault systems commonly change orientation along strike, composite basins as documented herein are likely to be associated with other strike-slip fault systems but are underrepresented in the literature.

It should be noted that our tectonic reconstruction approach is an over-simplification of a complex tectonic setting. The reconstruction assumes that: (1) the Pleistocene–Holocene slip rates along the Denali fault are reasonable approximations of the slip rates over the last 6.1 m.y.; (2) all strike-slip displacement can be accounted for on the main strand of the Kimball section of the Denali fault, when it is more likely that unrecognized subordinate parallel strike-slip faults as well as related thrust faults accommodated some of the inferred displacement; and (3) the fault junction between the Totschunda and eastern Denali fault has existed and has been stable over the past 6.1 m.y. These assumptions, hopefully, will be tested in future studies on this part of the Denali fault system.

## Neogene Regional Tectonics of the Upper Plate of the Southern Alaska Convergent Margin

Our analysis of the McCallum formation defines distinct stages of composite basin development and strike-slip displacement along the Denali fault system from ca. 6.1 Ma to the present. The age range determined for the McCallum formation coincides with widespread deformation and basin development across the southern Alaska convergent margin. To the west of the McCallum basin in the central Alaska Range, the Denali massif underwent rapid

exhumation (~1 km/m.y.) beginning at ca. 6 Ma (red star in Fig. 16; Plafker et al., 1992; Fitzgerald et al., 1993, 1995). The sedimentary record of the exhumation of Denali is recorded in the 1.2-km-thick Pliocene Nenana Gravel of the Tanana basin exposed north of the Alaska Range (Fig. 16; Wahrhaftig, 1987; Ridgway et al., 2007b; Brennan and Ridgway, 2015). On the south side of the central Alaska Range, Miocene and Pliocene deposition occurred in a wedge-top basin, the Peter Hills basin, along the Broad Pass thrust fault system (Fig. 16; Haeussler et al., 2017b). Southeast of the McCallum basin, along the southern margin of the upper plate, the St. Elias syntaxis is also marked by growth of high topography produced by focused, young exhumation of >5 km/m.y. from ca. 4 to 2 Ma (Fig. 16; Enkelmann et al., 2010, 2015). In this same general area, the hanging wall of the Chugach-St. Elias fault has been actively exhuming since 5 Ma, based on (U-Th)/He zircon analysis (Fig. 16; Berger et al., 2008). In the St. Elias region, the sedimentary record of Neogene deformation is a thick clastic wedge (~5 km) of Upper Miocene-Pleistocene synorogenic strata, known as the Yakataga Formation (e.g., Plafker, 1987; Lagoe et al., 1993; Plafker and Berg, 1994). In addition to the onshore marine record of rapid exhumation in the St. Elias region, the offshore record documents increased sedimentation in the Gulf of Alaska since ca. 5 Ma (Gulick et al., 2015). Southwest of the McCallum basin, in the Cook Inlet forearc basin, the sedimentary record of late Miocene-Pliocene deformation is inferred from the ~3.3-km-thick Sterling Formation (e.g., Flores et al., 2004; Finzel et al., 2011, 2015).

In addition to the development of young topography and deposition of synorogenic clastic wedges on the upper plate of the convergent margin, there was also increased late Miocene to Holocene volcanism in the Wrangell arc (Fig. 16). The Wrangell arc is located southeast of the McCallum basin and extends for ~500 km from southern Alaska to southwestern Yukon (Fig. 16; Richter, 1976; Richter et al., 1990; Skulski et al., 1991; Brueseke et al., 2019; Trop et al., 2022). The Wrangell arc has been active since ca. 30 Ma (Fig. 16; Richter et al., 1990; Preece and Hart, 2004; Brueseke et al., 2019). The late Miocene to present period of volcanism has resulted in the development of some of the highest, and largest by volume, volcanoes in North America (Fig. 16; Nye, 1983; Richter et al., 1990, 1994). The tephras documented in the McCallum basin were likely sourced from major Wrangell volcanoes that overlap in age with the deposition of the McCallum basin (ca. 6.1 Ma to present), such as Mount Blackburn (ca. 4 Ma).

The plate-boundary driving forces for regional Neogene deformation were likely related to subduction of the Yakutat slab, with its progressively thicker crust leading to active microplate collision along the southern Alaska convergent margin (Fig. 16; Plafker, 1987; Eberhart-Phillips et al., 2006; Christeson et al., 2010; Elliott et al., 2010; Finzel et al., 2011; Worthington et al., 2012; Elliott and Freymueller, 2020). An additional factor driving Neogene deformation may have been a shift in relative plate motion from a northwestern-directed vector motion to more northward-directed motion at ca. 6 Ma (Fig. 16; Cox and Engebretson, 1985; Engebretson et al., 1985; Fitzgerald et al., 1993, 1995; Wessel and Kroenke, 2007; Doubrovine and Tarduno, 2008). Our analysis of the McCallum basin illustrates a clear record of strike-slip displacement along

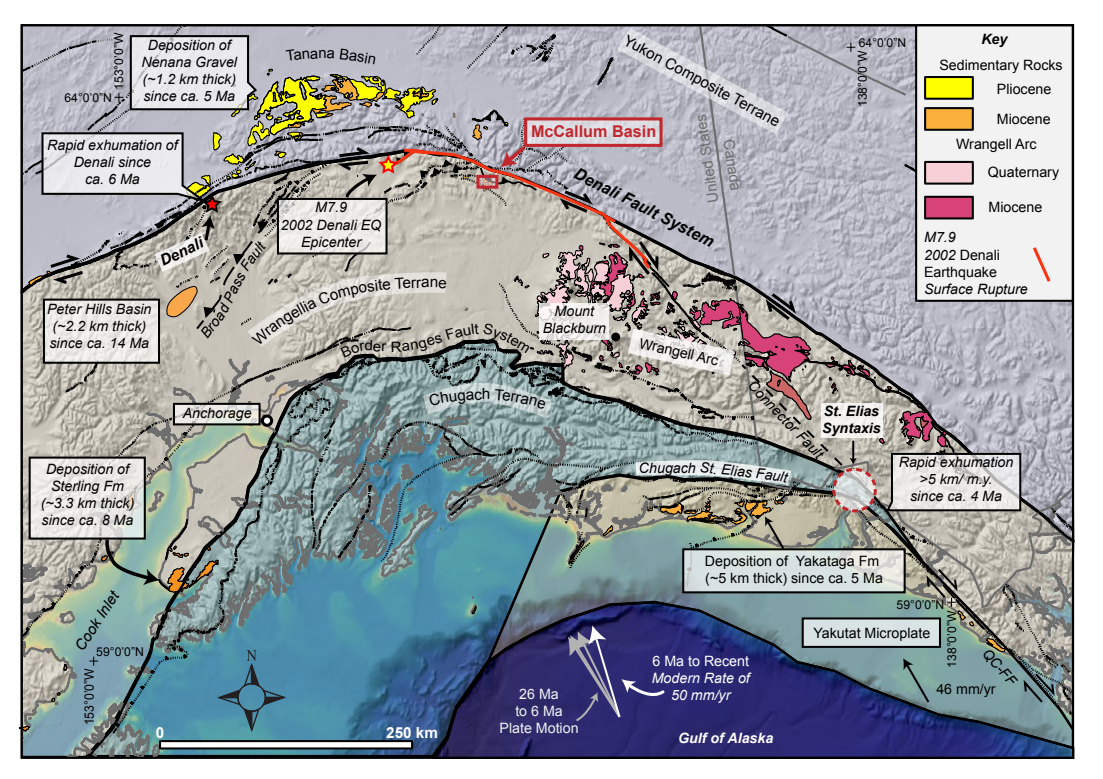


Figure 16. Basin development and related strikeslip deformation of the McCallum basin along the Denali fault system from ca. 6.17 Ma to present are part of a regional tectonic process that shapes the upper plate of the southern Alaska convergent margin. Deposition of thick clastic wedges starting in the late Miocene occurred in the Tanana basin (Nenana Gravel), Cook Inlet (Sterling Formation), the Peters Hill basin, and the Yakutat microplate (Yakataga Formation). Rapid cooling and exhumation of the Denali Massif and St. Elias syntaxis also occurred during this period, as well as volcanism in the Wrangell arc (e.g., Richter et al., 1990; Fitzgerald et al., 1993, 1995; Enkelmann et al., 2010). The 341 km surface rupture of the M 7.9 Denali earthquake is outlined by the red line (from Haeussler, 2009). Paleo-Pacific plate motion vectors are shown as gray arrows in three steps from 26 Ma to 17 Ma, from 17 Ma to 10 Ma, and from 10 Ma to 6 Ma as vectors become more northward, with the white arrow representing the 6 Ma to recent vector from Doubrovine and Tarduno (2008). Pacific plate and Yakutat microplate velocities are from Eberhart-Phillips et al. (2006) and Elliott et al. (2010). Geologic units are from Wilson et al. (2015) and Yukon Geological Survey (2020). QC-FF - Queen Charlotte-Fairweather fault. The background shaded relief is a global mosaic derived from bathymetric/topographic digital elevation models stewarded at the National Oceanic and Atmospheric Administration (NOAA) National Centers for Environmental Information (https://gis.ngdc.noaa.gov/arcgis/rest /services/DEM mosaics/DEM global mosaic hillshade/ImageServer).

the Denali fault system by ca. 6 Ma to the present. In general, we interpret this stage of strike-slip displacement and basin development to be a far-field response of the Denali fault to subduction of thicker crust of the Yakutat microplate along the plate boundary and changing plate-boundary conditions. Our findings build on a number of geologic, geophysical, and modeling studies that relate Neogene deformation in southern and central Alaska to flat slab subduction (Abers, 2008; Haeussler, 2008; Freymueller et al., 2008; Jadamec et al., 2013; Finzel et al., 2011, 2015).

The specific timing of strike-slip displacement along the Denali fault is unclear and warrants additional studies. Several previous studies have documented 300–400 km of Cretaceous and/or younger displacement based on correlation of interpreted offset Jurassic–Cretaceous sedimentary strata (Eisbacher, 1976; Nokleberg et al., 1985; Lowey, 1998; Fasulo et al., 2020). Due to the Mesozoic age of the offset markers, these important studies provide little insight into the specific timing of strike-slip displacement. The documentation of Eocene–Oligocene strike-slip basins along the Denali fault system led other previous studies to suggest that much of the total displacement may have

occurred during the Paleogene (e.g., Ridgway and DeCelles, 1993; Ridgway et al., 1999; Trop and Ridgway, 2007). Our analyses of the McCallum formation, combined with several other recent studies (Berkelhammer et al., 2019; Brueseke et al., 2019; Trop et al., 2019), indicate the importance of Neogene displacement along the Denali fault system. Additional studies are needed, but Neogene strike-slip displacement may represent a significant component of the total fault-slip record and will need to be incorporated into tectonic models and paleogeographic reconstructions to develop a more complete understanding of the geologic development of the southern Alaska convergent margin.

#### CONCLUSIONS

(1) The newly defined McCallum formation represents a period of active basin development and strike-slip displacement along the eastern Denali fault system from ca. 6.1 Ma to the present. Stratigraphic and geochronologic data define a 564-m-thick stratigraphic section for this formation that consists of a fine-grained, lacustrine-dominated lower member, and a coarse-grained, stream-dominated, alluvial-fan upper member. We interpret this stratigraphic transition to be a product of ~79–90 km of Neogene displacement along the Denali fault based on our palinspastic reconstruction. The formation of the basin along a transtensional section of the fault is interpreted to have started by ca. 6.1 Ma, and the basin was subsequently transported into a region of transpression by ca. 5 Ma. Displacement along the transpressional Kimball section of the Denali fault continues to the present and results in an active propagating thrust system that is deforming the northeastern margin of the McCallum basin. Previous studies of strike-slip basin development classify most basins into two end members: transtensional or transpressional. We interpret the McCallum basin as a composite strike-slip basin that bridges both end members. Composite basins are likely common along other strike-slip fault systems and warrant additional study.

- (2) Our analysis of the McCallum basin, combined with several other recent studies, indicates that ~79–90 km of the previously interpreted 300– 400 km of Cretaceous or younger dextral displacement on the Denali fault system are late Miocene and younger. Previous basin analysis studies placed an emphasis on Eocene–Oligocene displacement. The sedimentary record from the McCallum basin indicates that significant Neogene strike-slip displacement will now need to be incorporated into future tectonic reconstructions of the Denali fault system.
- (3) From a more regional perspective, the Neogene tectonics of southern Alaska are interpreted to be related to flat slab subduction of progressively thicker crust of the Yakutat microplate and a Pacific plate vector change. Much of the high topography and the related Neogene clastic wedges documented across the southern Alaska convergent margin are coeval with strike-slip displacement and basin development on the eastern Denali fault system; all of these upper-plate processes may be related to flat slab subduction.

#### **ACKNOWLEDGMENTS**

This research was supported by the National Science Foundation (EAR-1828737, Ridgway; EAR-1550034, Fitzgerald; and EAR-1434656, EAR-1550123, Benowitz). Allen received additional support from an Alaska Geological Society scholarship, a Geological Society of America research grant, the American Indian Science and Engineering Society, the Cearley Basin Analysis Fund, an Exxon-Mobil Geosciences scholarship, and graduate student research funds from the Department of Earth, Atmospheric, and Planetary Sciences at Purdue University. Allen also received support from the Sloan Indigenous Graduate Partnership Program at Purdue University. We benefited from discussions with Christopher Andronicos, Jeffrey Trop, Julie Elliott, Paul Layer, and Lucy Flesch. We also thank Basin Analysis team members: Mariah Romero, Lauren Colliver, Kim Davis, Cooper Fasulo, Tim Henderson, and Brandon Keough for constructive criticism during various stages of this research. Cooper Fasulo and Brandon Keough are thanked for assistance in field work. We appreciate the guidance from Arizona LaserChron Center staff scientists during U-Pb data acquisition. We thank Geosphere reviewers Peter Haeussler and Paul McCarthy, and Associate Editor Julie Dumoulin for helpful constructive comments that significantly improved the manuscript. Allen and Ridgway also thank Jeffrey Benowitz and Anna Liljedahl for lodging in Fairbanks and logistical support. Ridgway acknowledges the late Warren Nokleberg for first making him aware of the exposures along McCallum Creek.

#### REFERENCES CITED

- Abers, G.A., 2008, Orogenesis from subducting thick crust and evidence from Alaska, *in* Freymueller, J.T., et al., eds., ActiveTectonics and Seismic Potential of Alaska: American Geophysical Union Geophysical Monograph 179, p. 337–349, https://doi.org/10.1029/179GM19.
- Allmendinger, R.W., Cardozo, N., and Fisher, D., 2012, Structural Geology Algorithms: Vectors and Tensors in Structural Geology: Cambridge, UK, Cambridge University Press, 302 p.
- Barnes, P.M., Sutherland, R., and Delteil, J., 2005, Strike-slip structure and sedimentary basins of the southern Alpine fault, Fiordland, New Zealand: Geological Society of America Bulletin, v. 117, p. 411–435, https://doi.org/10.1130/B25458.1.
- Bemis, S.P., and Wallace, W.K., 2007, Neotectonic framework of the north-central Alaska Range foothills, in Ridgway, K.D., Trop, J.M., Glen, J.M.G., and O'Neill, J.M., eds., Tectonic Growth of a Collisional Continental Margin: Crustal Evolution of Southern Alaska: Geological Society of America Special Paper 431, p. 549–572, https://doi.org/10.1130/20072431(21).
- Bemis, S.P., Carver, G.A., and Koehler, R.D., 2012, The Quaternary thrust system of the northern Alaska Range: Geosphere, v. 8, p. 196–205, https://doi.org/10.1130/GES00695.1.
- Bemis, S.P., Weldon, R.J., and Carver, G.A., 2015, Slip partitioning along a continuously curved fault: Quaternary geologic controls on Denali fault system slip partitioning, growth of the Alaska Range, and the tectonics of south-central Alaska: Lithosphere, v. 7, p. 235–246, https:// doi.org/10.1130/L352.1.
- Benowitz, J.A., Layer, P.W., Armstrong, P., Perry, S.E., Haeussler, P.J., Fitzgerald, P.G., and Van-Laningham, S., 2011, Spatial variations in focused exhumation along a continental-scale strike-slip fault: The Denali fault of the eastern Alaska Range: Geosphere, v. 7, p. 455–467, https://doi.org/10.1130/GES00589.1.
- Berger, A.L., Spotila, J.A., Chapman, J.B., Pavlis, T.L., Enkelmann, E., Ruppert, N.A., and Buscher, J.T., 2008, Architecture, kinematics, and exhumation of a convergent orogenic wedge: A thermochronological investigation of tectonic-climatic interactions within the central St. Elias orogen, Alaska: Earth and Planetary Science Letters, v. 270, p. 13–24, https://doi.org/10.1016/j.epsl.2008.02.034.
- Berkelhammer, S.E., Brueseke, M.E., Benowitz, J.A., Trop, J.M., Davis, K., Layer, P.W., and Weber, M., 2019, Geochemical and geochronological records of tectonic changes along a flat-slab arc-transform junction: Circa 30 Ma to ca. 19 Ma Sonya Creek volcanic field, Wrangell arc, Alaska: Geosphere, v. 15, p. 1508–1538, https://doi.org/10.1130/GES02114.1.
- Bond, G.C., 1976, Geology of the Rainbow Mountain–Gulkana Glacier Area, Eastern Alaska Range, with Emphasis on Upper Paleozoic Strata: Alaska Division of Geological & Geophysical Surveys Geologic Report 45, 47 p., 3 sheets, https://doi.org/10.14509/373.
- Brennan, P.R.K., and Ridgway, K.D., 2015, Detrital zircon record of Neogene exhumation of the central Alaska Range: A far-field upper plate response to flat-slab subduction: Geological Society of America Bulletin, v. 127, p. 945–961, https://doi.org/10.1130/B31164.1.
- Brennan, P.R.K., Gilbert, H., and Ridgway, K.D., 2011, Crustal structure across the central Alaska Range: Anatomy of a Mesozoic collisional zone: Geochemistry Geophysics Geosystems, v. 12. Q04010. https://doi.org/10.1029/2011GC003519.
- Bridge, J.S., 2006, Fluvial facies models: Recent developments, in Posamentier, H.W., and Walker, R.G., eds., Facies Models Revisited: Society for Sedimentary Geology (SEPM) Special Publication 84. p. 85–170. https://doi.org/10.2110/pec.06.84.0085.
- Bridge, J.S., and Lunt, I.A., 2009, Depositional models of braided rivers, in Sambrook Smith, G.H., Best, J.L., Bristow, C.S., and Petts, G.E., eds., Braided Rivers: Process, Deposits, Ecology and Management: New York, John Wiley & Sons, Ltd., p. 11–50, https://doi.org/10.1002/9781444304374.ch2.
- Brocher, T.M., Fuis, G.S., Lutter, W.J., Christensen, N.I., and Ratchkovski, N.A., 2004, Seismic velocity models for the Denali fault zone along the Richardson Highway, Alaska: Bulletin of the Seismological Society of America, v. 94, p. S85–S106, https://doi.org/10.1785/0120040615.
- Brueseke, M.E., Benowitz, J.A., Trop, J.M., Davis, K.N., Berkelhammer, S.E., Layer, P.W., and Morter, B.K., 2019, The Alaska Wrangell arc: 30 Ma of subduction-related magmatism along a still active arc-transform junction: Terra Nova, v. 31, p. 59–66, https://doi.org/10.1111/ ter.12369.
- Burkett, C.A., Bemis, S.P., and Benowitz, J.A., 2016, Along-fault migration of the Mount McKinley restraining bend of the Denali fault defined by late Quaternary fault patterns and seismicity, Denali National Park & Preserve, Alaska: Tectonophysics, v. 693, p. 489–506, https://doi .org/10.1016/j.tecto.2016.05.009.
- Cardozo, N., and Allmendinger, R.W., 2013, Spherical projections with OSXStereonet: Computers & Geosciences, v. 51, p. 193–205, https://doi.org/10.1016/j.cageo.2012.07.021.

- Cassata, W.S., Singer, B.S., and Cassidy, J., 2008, Laschamp and Mono Lake geomagnetic excursions recorded in New Zealand: Earth and Planetary Science Letters, v. 268, p. 76–88, https://doi.org/10.1016/j.epsl.2008.01.009.
- Chen, W.-S., Ridgway, K.D., Horng, C.-S., Chen, Y.-G., Shea, K.-S., and Yeh, M.-G., 2001, Stratigraphic architecture, magnetostratigraphy, and incised-valley systems of the Pliocene–Pleistocene collisional marine foreland basin of Taiwan: Geological Society of America Bulletin, v. 113, p. 1249–1271, https://doi.org/10.1130/0016-7606(2001)113-1249:SAMAIV>2.0.CO;2.
- Choi, M., Eaton, D.W., and Enkelmann, E., 2021, Is the Eastern Denali fault still active?: Geology, v. 49, no. 6, p. 662–666, https://doi.org/10.1130/G48461.1.
- Christeson, G.L., Gulick, S.P.S., van Avendonk, H.J.A., Worthington, L.L., Reece, R.S., and Pavlis, T.L., 2010, The Yakutat terrane: Dramatic change in crustal thickness across the Transition fault, Alaska: Geology, v. 38, p. 895–898, https://doi.org/10.1130/G31170.1.
- Christie-Blick, N., and Biddle, K.T., 1985, Deformation and basin formation along strike-slip faults, in Biddle, K.T., and Christie-Blick, N., eds., Strike-Slip Deformation, Basin Formation, and Sedimentation: Society for Sedimentary Geology (SEPM) Special Publication 37, p. 1–34, https://doi.org/10.2110/pec.85.37.0001.
- Cogliati, S., Sherlock, S.C., Halton, A.M., Ebinghaus, A., Kelley, S.P., Jolley, D.W., and Barry, T.L., 2021, Expanding the toolbox for dating basaltic lava sequences: <sup>40</sup>Ar-<sup>30</sup>Ar dating of silicic volcanic glass from interbeds: Journal of the Geological Society [London], v. 178, p. jgs2019–jgs2207, https://doi.org/10.1144/jgs2019-207.
- Collinson, J.D., 1996, Alluvial sediments, in Reading, H.G., ed., Sedimentary Environments: Processes, Facies and Stratigraphy: Oxford, UK, Blackwell Scientific Publications, p. 37–81.
- Cowgill, E., Arrowsmith, J.R., Yin, A., Xiaofeng, W., and Zhengle, C., 2004, The Akato Tagh bend along the Altyn Tagh fault, northwest Tibet 2: Active deformation and the importance of transpression and strain hardening within the Altyn Tagh system: Geological Society of America Bulletin, v. 116, p. 1443–1464, https://doi.org/10.1130/B25360.1.
- Cox, A., and Engebretson, D., 1985, Change in motion of Pacific plate at 5 Myr BP: Nature, v. 313, p. 472–474, https://doi.org/10.1038/313472a0.
- Crone, A.J., Personius, S.F., Craw, P.A., Haeussler, P.J., and Staft, L.A., 2004, The Susitna Glacier thrust fault: Characteristics of surface ruptures on the fault that initiated the 2002 Denali fault earthquake: Bulletin of the Seismological Society of America, v. 94, p. S5–S22, https:// doi.org/10.1785/0120040619.
- Cross, R.S., and Freymueller, J.T., 2008, Evidence for and implications of a Bering plate based on geodetic measurements from the Aleutians and western Alaska: Journal of Geophysical Research–Solid Earth, v. 113, B07405, https://doi.org/0.1029/2007JB005136.
- Crowell, J.C., and Link, M.H., eds., 1982, Geologic History of Ridge Basin, Southern California: Los Angeles, California, Pacific Section, Society of Economic Paleontologists and Mineralogists (SEPM), 304 p.
- Denton, G.H., and Armstrong, R.L., 1969, Miocene–Pliocene glaciations in southern Alaska: American Journal of Science, v. 267, p. 1121–1142, https://doi.org/10.2475/ajs.267.10.1121.
- Dodds, C.J., 1992, Denali fault, in Gabrielse, H., and Yorath, C.J., eds., Geology of the Cordilleran Orogen in Canada: Boulder, Colorado, Geological Society of America, The Geology of North America, v. G2, p. 656–657, https://doi.org/10.1130/DNAG-GNA-G2.571.
- Doubrovine, P.V., and Tarduno, J.A., 2008, A revised kinematic model for the relative motion between Pacific oceanic plates and North America since the Late Cretaceous: Journal of Geophysical Research, v. 113, B12101, https://doi.org/10.1029/2008JB005585.
- Duk-Rodkin, A., Barendregt, R.W., Froese, D.G., Weber, F., Enkin, R., Rod Smith, I., Zazula, G.D., Waters, P., and Klassen, R., 2004, Timing and extent of Plio-Pleistocene glaciations in north-western Canada and east-central Alaska, in Ehlers, J., and Gibbard, P.L., eds., Quaternary Glaciations—Extent and Chronology: Amsterdam, Netherlands, Elsevier, Developments in Quaternary Sciences Volume 2, Part B, p. 313–345, https://doi.org/10.1016/S1571-0866(04)80206-9.
- Duk-Rodkin, A., Barendregt, R.W., and White, J.M., 2010, An extensive late Cenozoic terrestrial record of multiple glaciations preserved in the Tintina Trench of west-central Yukon: Stratigraphy, paleomagnetism, paleosols, and pollen: Canadian Journal of Earth Sciences, v. 47, p. 1003–1028, https://doi.org/10.1139/E10-060.
- Eberhart-Phillips, D., and 28 others, 2003, The 2002 Denali fault earthquake, Alaska: A large magnitude, slip-partitioned event: Science, v. 300, p. 1113–1118, https://doi.org/10.1126/science.1082703.
- Eberhart-Phillips, D., Christensen, D.H., Brocher, T.M., Hansen, R., Ruppert, N.A., Haeussler, P.J., and Abers, G.A., 2006, Imaging the transition from Aleutian subduction to Yakutat collision in central Alaska, with local earthquakes and active source data: Journal of Geophysical Research–Solid Earth, v. 111, B11303, https://doi.org/10.1029/2005JB004240.

- Eisbacher, G.H., 1976, Sedimentology of the Dezadeash flysch and its implications for strike-slip faulting along the Denali fault, YukonTerritory and Alaska: Canadian Journal of Earth Sciences, v. 13, p. 1495–1513, https://doi.org/10.1139/e76-157.
- Elliott, J., and Freymueller, J.T., 2020, A block model of present-day kinematics of Alaska and western Canada: Journal of Geophysical Research–Solid Earth, v. 125, p. e2019JB018378, https://doi.org/10.1029/2019JB018378.
- Elliott, J.L., Larsen, C.F., Freymueller, J.T., and Motyka, R.J., 2010, Tectonic block motion and glacial isostatic adjustment in southeast Alaska and adjacent Canada constrained by GPS measurements: Journal of Geophysical Research–Solid Earth, v. 115, B09407, https://doi.org/10.1029/2009JB007139.
- Engebretson, D.C., Cox, A., and Gordon, R.G., 1985, Relative Motions Between Oceanic and Continental Plates in the Pacific Basin: Geological Society of America Special Paper 206, 59 p., https://doi.org/10.1130/SPE206-p1.
- Enkelmann, E., Zeitler, P.K., Garver, J.I., Pavlis, T.L., and Hooks, B.P., 2010, The thermochronological record of tectonic and surface process interaction at the Yakutat–North American collision zone in southeast Alaska: American Journal of Science, v. 310, p. 231–260, https://doi.org/10.2475/04.2010.01.
- Enkelmann, E., Koons, P.O., Pavlis, T.L., Hallet, B., Barker, A., Elliott, J., Garver, J.I., Gulick, S.P.S., Headley, R.M., Pavlis, G.L., Ridgway, K.D., Ruppert, N., and Avendonk, H.J.A.V., 2015, Cooperation among tectonic and surface processes in the St. Elias Range, Earth's highest coastal mountains: Geophysical Research Letters, v. 42, p. 5838–5846, https://doi.org/10.1002/2015GL064727.
- Fasulo, C.R., Ridgway, K.D., and Trop, J.M., 2020, Detrital zircon geochronology and Hf isotope geochemistry of Mesozoic sedimentary basins in south-central Alaska: Insights into regional sediment transport, basin development, and tectonics along the NW Cordilleran margin: Geosphere, v. 16, no. 5, p. 1125–1152, https://doi.org/10.1130/GES02221.1
- Ferrians, O.J., Jr., and Schmoll, H.R., 1957, Extensive proglacial lake of Wisconsin age in the Copper River Basin, Alaska: Geological Society of America Bulletin, v. 68, p. 1726.
- Finzel, E.S., Trop, J.M., Ridgway, K.D., and Enkelmann, E., 2011, Upper plate proxies for flatslab subduction processes in southern Alaska: Earth and Planetary Science Letters, v. 303, p. 348–360, https://doi.org/10.1016/j.epsl.2011.01.014.
- Finzel, E.S., Ridgway, K.D., and Trop, J.M., 2015, Provenance signature of changing plate boundary conditions along a convergent margin: Detrital record of spreading-ridge and flat-slab subduction processes, Cenozoic forearc basins, Alaska: Geosphere, v. 11, p. 823–849, https://doi.org/10.1130/GES01029.1.
- Fisher, J.A., Nichols, G.J., and Waltham, D.A., 2007, Unconfined flow deposits in distal sectors of fluvial distributary systems: Examples from the Miocene Luna and Huesca systems, northern Spain: Sedimentary Geology, v. 195, p. 55–73, https://doi.org/10.1016/j.sedgeo.2006.07.005.
- Fitzgerald, P.G., Stump, E., and Redfield, T.F., 1993, Late Cenozoic uplift of Denali and its relation to relative plate motion and fault morphology: Science, v. 259, p. 497–499, https://doi.org/10.1126/science.259.5094.497.
- Fitzgerald, P.G., Sorkhabi, R.B., Redfield, T.F., and Stump, E., 1995, Uplift and denudation of the central Alaska Range: A case study in the use of apatite fission track thermochronology to determine absolute uplift parameters: Journal of Geophysical Research–Solid Earth, v. 100, p. 20175–20191, https://doi.org/10.1029/95JB02150.
- Fitzgerald, P.G., Roeske, S.M., Benowitz, J.A., Riccio, S.J., Perry, S.E., and Armstrong, P.A., 2014, Alternating asymmetric topography of the Alaska Range along the strike-slip Denali fault: Strain partitioning and lithospheric control across a terrane suture zone: Tectonics, v. 33, p. 1519–1533, https://doi.org/10.1002/2013TC003432.
- Fletcher, H.J., and Freymueller, J.T., 2003, New constraints on the motion of the Fairweather fault, Alaska, from GPS observations: Geophysical Research Letters, v. 30, 1139, https://doi.org/10.1029/2002GL016476.
- Flores, R.M., Stricker, G.D., and Kinney, S.A., 2004, Alaska Coal Geology, Resources, and Coal-bed Methane Potential: U.S. Geological Survey Digital Data Series 77, 140 p., https://doi.org/10.3133/ds77.
- Fouch, T.D., and Dean, W.E., 1982, Lacustrine and associated clastic depositional environments, in Scholle, P.A., and Spearing, D., eds., Sandstone Depositional Environments: American Association of Petroleum Geologists Memoir 31, p. 87–101, https://doi.org/10.1306/M31424C5.
- Freymueller, J.T., Woodard, H., Cohen, H.S., Cross, R., Elliott, J., Larsen, C., Hreinsdottir, S., and Zweck, C., 2008, Active deformation processes in Alaska, based on 15 years of GPS measurements, in Freymueller, J.T., et al., eds., Active Tectonics and Seismic Potential of Alaska: American Geophysical Union Geophysical Monograph 179, p. 1–42, https://doi.org/10.1029/GM179.

- Fuis, G.S., Moore, T.E., Plafker, G., Brocher, T.M., Fisher, M.A., Mooney, W.D., Nokleberg, W.J., Page, R.A., Beaudoin, B.C., Christensen, N.I., Levander, A.R., Lutter, W.J., Saltus, R.W., and Ruppert, N.A., 2008, Trans-Alaska Crustal Transect and continental evolution involving subduction underplating and synchronous foreland thrusting: Geology, v. 36, p. 267–270, https:// doi.org/10.1130/G24257A.1.
- Ghinassi, M., and lelpi, A., 2016, Morphodynamics and facies architecture of streamflow-dominated, sand-rich alluvial fans, Pleistocene Upper Valdarno Basin, Italy, in Ventra, D., Clarke, L.E., eds., Geology and Geomorphology of Alluvial and Fluvial Fans: Terrestrial and Planetary Perspectives: Geological Society [London] Special Publication 440, p. 175–200, https://doi.org/10.1144/SP440.1.
- Gillis, R.J., Fitzgerald, P.G., Ridgway, K.D., Keough, B.M., Benowitz, J.A., and Allen, W.K., 2019, Overview of the New 1:25,000-Scale Geologic Mapping of the McCallum–Slate Creek fault system, Eastern Alaska Range, Alaska: Alaska Division of Geological & Geophysical Surveys Preliminary Interpretive Report 2018–3, 10 p., https://doi.org/10.14509/30136.
- Godin, P.D., 1991, Fining-upward cycles in the sandy braided-river deposits of the Westwater Canyon Member (Upper Jurassic), Morrison Formation, New Mexico: Sedimentary Geology, v. 70, p. 61–82, https://doi.org/10.1016/0037-0738(91)90066-M.
- Grantz, A., 1966, Strike-SLIP FAULTS in Alaska: U.S. Geological Survey Open-File Report 66–53, 82 p., https://doi.org/10.3133/ofr6653.
- Gulick, S.P.S., and 36 others, 2015, Mid-Pleistocene climate transition drives net mass loss from rapidly uplifting St. Elias Mountains, Alaska: Proceedings of the National Academy of Sciences of the United States of America, v. 112. p. 15042–15047, https://doi.org/10.1073/pnas.1512549112.
- Haeussler, P.J., 2008, An overview of the neotectonics of interior Alaska: Far-field deformation from the Yakutat microplate collision, in Freymueller, J.T., Haeussler, P.J., Wesson, R.L., and Ekström, G., eds., Active Tectonics and Seismic Potential of Alaska: American Geophysical Union Geophysical Monograph 179, p. 83–108, https://doi.org/10.1029/179GM05.
- Haeussler, P.J., 2009, Surface Rupture Map of the 2002 M7.9 Denali Fault Earthquake, Alaska; Digital Data: U.S. Geological Survey Data Series 422, http://pubs.usgs.gov/ds/422/.
- Haeussler, P.J., Schwartz, D.P., Dawson, T.E., Stenner, H.D., Lienkaemper, J.J., Sherrod, B., Cinti, F.R., Montone, P., Craw, P.A., Crone, A.J., and Personius, S.F., 2004, Surface rupture and slip distribution of the Denali and Totschunda faults in the 3 November 2002 M 7.9 earth-quake, Alaska: Bulletin of the Seismological Society of America, v. 94, p. S23–S52, https://doi.org/10.1785/0120040626.
- Haeussler, P.J., Matmon, A., Schwartz, D.P., and Seitz, G.G., 2017a, Neotectonics of interior Alaska and the late Quaternary slip rate along the Denali fault system: Geosphere, v. 13, p. 1445–1463, https://doi.org/10.1130/GES01447.1.
- Haeussler, P.J., Saltus, R.W., Stanley, R.G., Ruppert, N., Lewis, K., Karl, S.M., and Bender, A., 2017b, The Peters Hills basin, a Neogene wedge-top basin on the Broad Pass thrust fault, south-central Alaska: Geosphere, v. 13, p. 1464–1488, https://doi.org/10.1130/GES01487.1.
- Hanson, L.G., 1963, Bedrock Geology of the Rainbow Mountain Area, Alaska Range, Alaska: Alaska Division of Mines and Minerals Geologic Report 2, 82 p., 2 sheets, https://doi.org/10.14509/331.
- Ingersoll, R.V., 2011, Tectonics of sedimentary basins, with revised nomenclature, in Busby, C.J., and Azor, A., eds., Tectonics of Sedimentary Basins: New York, John Wiley & Sons, Ltd., p. 1–43, https://doi.org/10.1002/9781444347166.ch1.
- Jadamec, M.A., Billen, M.I., and Roeske, S.M., 2013, Three-dimensional numerical models of flat slab subduction and the Denali fault driving deformation in south-central Alaska: Earth and Planetary Science Letters, v. 376, p. 29–42, https://doi.org/10.1016/j.epsl.2013.06.009.
- Jo, H.R., Rhee, C.W., and Chough, S.K., 1997, Distinctive characteristics of a streamflow-dominated alluvial fan deposit: Sanghori area, Kyongsang Basin (Early Cretaceous), southeastern Korea: Sedimentary Geology, v. 110, p. 51–79, https://doi.org/10.1016/S0037-0738(96)00083-8.
- Kunk, M.J., 1995, <sup>40</sup>Ar/<sup>58</sup>Ar Age-Spectrum Data for Hornblende, Plagioclase and Biotite from Tephras Collected at Dan Creek and McCallum Creek, Alaska, and in the Klondike Placer District near Dawson, Yukon Territory, Canada: U.S. Geological Survey Open-File Report 95–217A, 52 p., https://doi.org/10.3133/ofr95217A.
- Lagoe, M.B., Eyles, C.H., Eyles, N., and Hale, C., 1993, Timing of late Cenozoic tidewater glaciation in the far North Pacific: Geological Society of America Bulletin, v. 105, p. 1542–1560, https://doi.org/10.1130/0016-7606(1993)105<1542:TOLCTG>2.3.CO;2.
- Lease, R.O., Haeussler, P.J., and O'Sullivan, P., 2016, Changing exhumation patterns during Cenozoic growth and glaciation of the Alaska Range: Insights from detrital thermochronology and geochronology: Tectonics, v. 35, p. 934–955, https://doi.org/10.1002/2015TC004067.
- Lesh, M.E., and Ridgway, K.D., 2007, Geomorphic evidence of active transpressional deformation in the Tanana foreland basin, south-central Alaska, in Ridgway, K.D., Trop, J.M., Glen, J.M.G.,

- and O'Neill, J.M. eds., Tectonic Growth of a Collisional Continental Margin: Crustal Evolution of Southern Alaska: Geological Society of America Special Paper 431, p. 573–592, https://doi.org/10.1130/2007.2431(22).
- Lowey, G.W., 1998, A new estimate of the amount of displacement on the Denali fault system based on the occurrence of carbonate megaboulders in the Dezadeash Formation (Jura-Cretaceous), Yukon, and the Nutzotin Mountains sequence (Jura-Cretaceous), Alaska: Bulletin of Canadian Petroleum Geology, v. 46, p. 379–386.
- Lunt, I.A., and Bridge, J.S., 2004, Evolution and deposits of a gravelly braid bar, Sagavanirktok River, Alaska: Sedimentology, v. 51, p. 415–432, https://doi.org/10.1111/j.1365-3091.2004.00628.x.
- Mann, P., 2007, Global catalogue, classification and tectonic origins of restraining- and releasing bends on active and ancient strike-slip fault systems, in Cunningham, W.D., and Mann, P., eds., Tectonics of Strike-Slip Restraining and Releasing Bends: Geological Society [London] Special Publication 290, p. 13–142, https://doi.org/10.1144/SP290.2.
- Mann, P., Hempton, M.R., Bradley, D.C., and Burke, K., 1983, Development of pull-apart basins: The Journal of Geology, v. 91, p. 529–554, https://doi.org/10.1086/628803.
- Marechal, A., Ritz, J.-F., Ferry, M., Mazzotti, S., Blard, P.-H., Braucher, R., and Saint-Carlier, D., 2018, Active tectonics around the Yakutat indentor: New geomorphological constraints on the eastern Denali, Totschunda and Duke River faults: Earth and Planetary Science Letters, v. 482, p. 71–80, https://doi.org/10.1016/j.epsl.2017.10.051.
- Matmon, A., Schwartz, D.P., Haeussler, P.J., Finkel, R., Lienkaemper, J.J., Stenner, H.D., and Dawson, T., 2006, Denali fault slip rates and Holocene–late Pleistocene kinematics of central Alaska: Geology, v. 34, p. 645–648, https://doi.org/10.1130/G22361.1.
- McCabe, P.J., 1985, Depositional environments of coal and coal-bearing strata, *in* Rahmani, R.A., and Flores, R.M., eds., Sedimentology of Coal and Coal-Bearing Sequences: New York, John Wiley & Sons, Ltd, p. 11–42, https://doi.org/10.1002/9781444303797.ch2.
- Mériaux, A.-S., Sieh, K., Finkel, R.C., Rubin, C.M., Taylor, M.H., Meltzner, A.J., and Ryerson, F.J., 2009, Kinematic behavior of southern Alaska constrained by westward decreasing postglacial slip rates on the Denali fault, Alaska: Journal of Geophysical Research–Solid Earth, v. 114, B03404, https://doi.org/10.1029/2007.JB005053.
- Miall, A., 2010, Alluvial deposits, in James, N.P., and Dalrymple, R.W., eds., Facies Models 4: St. John's, Newfoundland, Canada, Geological Association of Canada, p. 105–137.
- Morin, R.L., and Glen, J.M.G., 2003, Principal Facts for 408 Gravity Stations in the Vicinity of the Talkeetna Mountains, South-Central Alaska: U.S. Geological Survey Open-File Report 2003–27, 21 p., https://doi.org/10.3133/ofr0327.
- Nichols, G.J., and Fisher, J.A., 2007, Processes, facies and architecture of fluvial distributary system deposits: Sedimentary Geology, v. 195, p. 75–90, https://doi.org/10.1016/j.sedgeo.2006.07.004.
- Nokleberg, W.J., Albert, N.R.D., Bond, G.C., Herzon, P.L., Miyaoka, R.T., Nelson, W.H., Richter, D.H., Smith, T.E., Stout, J.H., Yeend, W., and Zehner, R.E., 1982, Geologic Map of the Southern Part of Mount Hayes Quadrangle, Alaska: U.S. Geological Survey Open-File Report 82–52, 26 p., https://doi.org/10.3133/oft8252.
- Nokleberg, W.J., Jones, D.L., and Silberling, N.J., 1985, Origin and tectonic evolution of the Maclaren and Wrangellia terranes, eastern Alaska Range, Alaska: Geological Society of America Bulletin, v. 96, p. 1251–1270, https://doi.org/10.1130/0016-7606(1985)96<1251:OATEOT >2.0.CO:2.
- Nokleberg, W.J., Aleinikoff, J.N., Lange, I.M., Silva, S.R., Miyaoka, R.T., Schwab, C.E., Zehner, R.E., Bond, G.C., Richter, D.H., Smith, T.E., and Stout, J.H., 1992a, Preliminary Geologic Map of the Mount Hayes Quadrangle, Eastern Alaska Range, Alaska: U.S. Geological Survey Open-File Report 92–594, 39 p., https://doi.org/10.3133/off92594.
- Nokleberg, W.J., Aleinikoff, J.N., Dutro, J.T., Jr., Lanphere, M.A., Silberling, N.J., Silva, S.R., Smith, T.E., and Turner, D.L., 1992b, Map, Tables, and Summary of Fossil and Isotopic Age Data, Mount Hayes Quadrangle, Eastern Alaska Range, Alaska: U.S. Geological Survey Miscellaneous Field Studies Map Report 1996D, 43 p., https://doi.org/10.3133/mf1996D.
- Nokleberg, W.J., Plafker, G., and Wilson, F.H., 1994, Geology of south-central Alaska, in Plafker, G., and Berg, H.C., eds., The Geology of Alaska: Boulder, Colorado, Geological Society of America, The Geology of North America, v. G-1, p. 311–366, https://doi.org/10.1130/DNAG-GNA.G1.311
- Nokleberg, W.J., Aleinikoff, J.N., Bond, G.C., Ferrians, O.J., Jr., Herzon, P.L., Lange, I.M., Miyaoka, R.T., Richter, D.H., Schwab, C.E., Silva, S.R., Smith, T.E., and Zehner, R.E., 2015, Geologic Maps of the Eastern Alaska Range, Alaska: Alaska Division of Geological & Geophysical Surveys Report 2015–6, 64 p., scale 1:63,360, https://doi.org/10.14509/29444.
- Nye, C.J., 1983, Petrology and Geochemistry of Okmok and Wrangell Volcanoes, Alaska [Ph.D. dissertation]: Santa Cruz, California, University of California–Santa Cruz, 208 p., and maps.

- Péwé, T.L., 1987, Delta River area, Alaska Range, Alaska, in Hill, M.L., ed., Cordilleran Section of the Geological Society of America Centennial Field Guide 1: Boulder, Colorado, Geological Society of America, p. 451–456, https://doi.org/10.1130/0-8137-5401-1.451.
- Plafker, G., 1987, Regional geology and petroleum potential of the northern Gulf of Alaska continental margin, in Scholl, D.W., Grantz, A., and Vedder, J.G., eds., Geology and Resource Potential of the Continental Margin of Western North America and Adjacent Ocean Basins—Beaufort Sea to Baja California: Circum-Pacific Council for Energy and Mineral Resources Earth Science Series 6, p. 229–268.
- Plafker, G., and Berg, H.C., 1994, Overview of the geology and tectonic evolution of Alaska, in Plafker, G., and Berg, H.C., eds., The Geology of Alaska: Boulder, Colorado, Geological Society of America, The Geology of North America, v. G-1, p. 989–1021, https://doi.org/10.1130/DNAG-GNA-G1.989.
- Plafker, G., Naeser, C.W., Zimmermann, R.A., Lull, J.S., and Hudson, T., 1992, Cenozoic uplift history of the Mount McKinley area in the central Alaska Range based on fission-track dating, in Bradley, D.C., and Dusel-Bacon, C., eds., Geologic Studies in Alaska by the U.S. Geological Survey, 1991: U.S. Geological Survey Bulletin 2041, p. 202–212, https://dggs.alaska.gov/webpubs/usgs/b/text/b2041.pdf.
- Preece, S.J., and Hart, W.K., 2004, Geochemical variations in the <5 Ma Wrangell volcanic field, Alaska: Implications for the magmatic and tectonic development of a complex continental arc system: Tectonophysics, v. 392, p. 165–191, https://doi.org/10.1016/j.tecto.2004.04.011.
- Reading, H.G., 1980, Characteristics and recognition of strike-slip fault systems, in Ballance, P.F., and Reading, H.G., eds., Sedimentation in Oblique-Slip Mobile Zones: NewYork, John Wiley & Sons, Ltd., p. 7–26, https://doi.org/10.1002/9781444303735.ch2.
- Reed, B.L., and Lanphere, M.A., 1974, Offset plutons and history of movement along the McKinley segment of the Denali fault system, Alaska: Geological Society of America Bulletin, v. 85, p. 1883–1892, https://doi.org/10.1130/0016-7606(1974)85</ri>
- Regan, S.P., Benowitz, J.A., and Holland, M.E., 2020, A plutonic brother from another magma mother: Disproving the Eocene Foraker-McGonagall pluton piercing point and implications for long-term slip on the Denali fault: Terra Nova, v. 32, p. 66–74, https://doi.org/10.1111/ter.12437.
- Renaut, R.W., and Gierlowski-Kordesch, E.H., 2010, Lakes, in James, N.P., and Dalrymple, R.W., eds., Facies Models 4: St. John's, Newfoundland Canada, Geological Association of Canada, p. 541–575.
- Riccio, S.J., Fitzgerald, P.G., Benowitz, J.A., and Roeske, S.M., 2014, The role of thrust faulting in the formation of the eastern Alaska Range: Thermochronological constraints from the Susitna Glacier thrust fault region of the intracontinental strike-slip Denali fault system: Tectonics, v. 33, p. 2195–2217, https://doi.org/10.1002/2014TC003646.
- Richter, D.H., 1976, Geologic Map of the Nabesna Quadrangle, Alaska: U.S. Geological Survey IMAP Report 932, scale 1:250,000, https://doi.org/10.3133/i932.
- Richter, D.H., and Matson, N.A., 1971, Quaternary faulting in the eastern Alaska Range: Geological Society of America Bulletin, v. 82, p. 1529–1540, https://doi.org/10.1130/0016-7606(1971) 82[1529:QFITEA]2.0.CO;2.
- Richter, D.H., Smith, J.G., Lanphere, M.A., Dalrymple, G.B., Reed, B.L., and Shew, N., 1990, Age and progression of volcanism, Wrangell volcanic field, Alaska: Bulletin of Volcanology, v. 53, p. 29–44, https://doi.org/10.1007/BF00680318.
- Richter, D.H., Moll-Stalcup, E.J., Miller, T.P., Lanphere, M.A., Dalrymple, G.B., and Smith, R.L., 1994, Eruptive history and petrology of Mount Drum volcano, Wrangell Mountains, Alaska: Bulletin of Volcanology, v. 56, p. 29–46, https://doi.org/10.1007/BF00279727.
- Ridgway, K.D., and DeCelles, P.G., 1993, Stream-dominated alluvial fan and lacustrine depositional systems in Cenozoic strike-slip basins, Denali fault system, Yukon Territory, Canada: Sedimentology, v. 40, p. 645–666, https://doi.org/10.1111/j.1365-3091.1993.tb01354.x.
- Ridgway, K.D., Sweet, A.R., and Cameron, A.R., 1995, Climatically induced floristic changes across the Eocene-Oligocene transition in the northern high latitudes, Yukon Territory, Canada: Geological Society of America Bulletin, v. 107, p. 676–696, https://doi.org/10.1130/0016-7606(1995) 107-0676:CIFCAT>2.3.CO:2.
- Ridgway, K.D., Trop, J.M., and Jones, D.E., 1999, Petrology and provenance of the Neogene Usibelli Group and Nenana Gravel: Implications for the denudation history of the central Alaska Range: Journal of Sedimentary Research, v. 69, p. 1262–1275, https://doi.org/10.2110/jsr 69 1262
- Ridgway, K.D., Trop, J.M., and Sweet, A.R., 2000, Stratigraphy, depositional systems, and age of the Tertiary White Mountain basin, Denali fault system, southwestern Alaska, in Pinney, D.S., and Davis, P.K., eds., Short Notes on Alaska Geology 1999: Alaska Division of Geological & Geophysical Surveys Professional Report 119F, p. 77–84. https://doi.org/10.14509/2688.

- Ridgway, K.D., Trop, J., Nokleberg, W., Davidson, C., and Eastham, K., 2002, Mesozoic and Cenozoic tectonics of the eastern and central Alaska Range: Progressive basin development and deformation in a suture zone: Geological Society of America Bulletin, v. 114, p. 1480–1504, https://doi.org/10.1130/0016-7606(2002)114<1480:MACTOT>-2.0.CO;2.
- Ridgway, K.D., Trop, J.M., Glen, J.M.G., and O'Neill, J.M., eds., 2007a, Tectonic Growth of a Collisional Continental Margin: Crustal Evolution of Southern Alaska: Geological Society of America Special Paper 431, 658 p., https://doi.org/10.1130/SPE431.
- Ridgway, K.D., Thoms, E.E., Layer, P.W., Lesh, M.E., White, J.M., and Smith, S.V., 2007b, Neogene transpressional foreland basin development on the north side of the central Alaska Range, Usibelli Group and Nenana Gravel, Tanana basin, in Ridgway, K.D., Trop, J.M., Glen, J.M.G., and O'Neill, J.M., eds., Tectonic Growth of a Collisional Continental Margin: Crustal Evolution of Southern Alaska: Geological Society of America Special Paper 431, p. 507–547, https://doi.org/10.1130/2007.2431(20).
- Roddick, J.C., 1978, The application of isochron diagrams in <sup>40</sup>Ar-<sup>39</sup>Ar dating: A discussion: Earth and Planetary Science Letters, v. 41, p. 233–244, https://doi.org/10.1016/0012-821X(78)90014-6.
- Roddick, J.C., Cliff, R.A., and Rex, D.C., 1980, The evolution of excess argon in alpine biotites—A <sup>40</sup>Ar-<sup>39</sup>Ar analysis: Earth and Planetary Science Letters, v. 48, p. 185–208, https://doi.org/10.1016/0012-821X(80)90181-8.
- Romero, M.C., Ridgway, K.D., and Gehrels, G.E., 2020, Geology, U-Pb geochronology, and Hf isotope geochemistry across the Mesozoic Alaska Range suture zone (south-central Alaska): Implications for Cordilleran collisional processes and tectonic growth of North America: Tectonics. v. 39. p. e2019TC005946. https://doi.org/10.1029/2019TC005946.
- Rust, B.R., and Jones, B.G., 1987, The Hawkesbury Sandstone south of Sydney, Australia: Triassic analogue for the deposit of a large, braided river: Journal of Sedimentary Research, v. 57, p. 222–233, https://doi.org/10.1306/212F8AEE-2B24-11D7-8648000102C1865D.
- Ryan, W.B.F., Carbotte, S.M., Coplan, J.O., O'Hara, S., Melkonian, A., Arko, R., Weissel, R.A., Ferrini, V., Goodwillie, A., Nitsche, F., Bonczkowski, J., and Zemsky, R., 2009, Global Multi-Resolution Topography synthesis: Geochemistry Geophysics Geosystems, v. 10, Q03014, https://doi.org/10.1029/2008GC002332.
- Sambrook Smith, G.H., Ashworth, P.J., Best, J.L., Woodward, J., and Simpson, C.J., 2006, The sedimentology and alluvial architecture of the sandy braided South Saskatchewan River, Canada: Sedimentology, v. 53, p. 413–434, https://doi.org/10.1111/j.1365-3091.2005.00769.x.
- Schneider, C.L., Hummon, C., Yeats, R.S., and Huftile, G.L., 1996, Structural evolution of the northern Los Angeles basin, California, based on growth strata: Tectonics, v. 15, p. 341–355, https://doi.org/10.1029/95TC02523.
- Schnurrenberger, D., Russell, J., and Kelts, K., 2003, Classification of lacustrine sediments based on sedimentary components: Journal of Paleolimnology, v. 29, p. 141–154, https://doi .org/10.1023/A:1023270324800.
- Schumm, S.A., Mosley, M.P., and Weaver, W., 1987, Experimental Fluvial Geomorphology: New York, Wiley, 413 p., https://www.osti.gov/biblio/6211294.
- Schwartz, D.P., Haeussler, P.J., Seitz, G.G., and Dawson, T.E., 2012, Why the 2002 Denali fault rupture propagated onto the Totschunda fault: Implications for fault branching and seismic hazards: Journal of Geophysical Research–Solid Earth, v. 117, B11304, https://doi.org /10.1029/2011JB008918.
- Sharp, W.D., and Renne, P.R., 2005, The <sup>40</sup>Ar/<sup>39</sup>Ar dating of core recovered by the Hawaii Scientific Drilling Project (phase 2), Hilo, Hawaii: Geochemistry Geophysics Geosystems, v. 6, Q04G17, https://doi.org/10.1029/2004GC000846.
- Skulski, T., Francis, D., and Ludden, J., 1991, Arc-transform magmatism in the Wrangell volcanic belt: Geology, v. 19, p. 11–14, https://doi.org/10.1130/0091-7613(1991)019<0011:ATMITW>2.3.CO;2.
- Śliwiński, M., Bąbel, M., Nejbert, K., Olszewska-Nejbert, D., Gąsiewicz, A., Schreiber, B., Benowitz, J., and Layer, P., 2012, Badenian–Sarmatian chronostratigraphy in the Polish Carpathian foredeep: Palaeogeography, Palaeoclimatology, Palaeoecology, v. 326–328, p. 12–29, https://doi.org/10.1016/j.palaeo.2011.12.018.
- Smith, G.A., 1991, Facies sequences and geometries in continental volcaniclastic sediments, in Fisher, R.V., and Smith, G.A. eds., Sedimentation in Volcanic Settings: Society for Sedimentary Geology (SEPM) Special Publication 45, p. 109–121, https://doi.org/10.2110 /pec.91.45.0109.
- Smith, N.D., 1974, Sedimentology and bar formation in the Upper Kicking Horse River, a braided outwash stream: The Journal of Geology, v. 82, p. 205–223, https://doi.org/10.1086/627959.
- St. Amand, P., 1957, Geological and geophysical synthesis of the tectonics of portions of British Columbia, the Yukon Territory, and Alaska: Geological Society of America Bulletin, v. 68, p. 1343–1370, https://doi.org/10.1130/0016-7606(1957)68[1343:GAGSOT]2.0.CO;2.

- Stout, J.H., 1976, Geology of the Eureka Creek Area, East-Central Alaska Range: Alaska Division of Geological & Geophysical Surveys Geologic Report 46, 32 p., 1 sheet, scale 1:63,360, http://doi.org/10.14509/374.
- Stout, J.H., and Chase, C.G., 1980, Plate kinematics of the Denali fault system: Canadian Journal of Earth Sciences, v. 17, p. 1527–1537, https://doi.org/10.1139/e80-160.
- Sturm, M., and Matter, A., 1978, Turbidites and varves in Lake Brienz (Switzerland): Deposition of clastic detritus by density currents, in Matter, A., and Tucker, M.E., eds., Modern and Ancient Lake Sediments: New York, John Wiley & Sons, Ltd., p. 147–168, https://doi.org/10.1002/9781444303698.ch8.
- Sylvester, A.G., and Smith, R.R., 1976, Tectonic transpression and basement-controlled deformation in San Andreas fault zone, Salton Trough, California: American Association of Petroleum Geologists Bulletin, v. 60, p. 2081–2102, https://doi.org/10.1306/C1EA3A73-16C9-11D7-8645000102C1865D.
- Talbot, M.R., and Allen, P.A., 1996, Lakes, in Reading, H.G., ed., Sedimentary Environments: Processes, Facies and Stratigraphy (3rd ed.): Oxford, UK, Blackwell Science, p. 83–124.
- Trop, J.M., and Ridgway, K.D., 2007, Mesozoic and Cenozoic tectonic growth of southern Alaska: A sedimentary basin perspective, in Ridgway, K.D., Trop, J.M., Glen, J.M.G., and O'Neill, J.M., eds., Tectonic Growth of a Collisional Continental Margin: Crustal Evolution of Southern Alaska: Geological Society of America Special Paper 431, p. 55–94, https://doi.org/10.1130/2007.2431(04).
- Trop, J.M., Hart, W.K., Snyder, D., and Idleman, B., 2012, Miocene basin development and volcanism along a strike-slip to flat-slab subduction transition: Stratigraphy, geochemistry, and geochronology of the central Wrangell volcanic belt, Yakutat–North America collision zone: Geosphere, v. 8, p. 805–834, https://doi.org/10.1130/GES00762.1.
- Trop, J.M., Benowitz, J., Cole, R.B., and O'Sullivan, P., 2019, Cretaceous to Miocene magmatism, sedimentation, and exhumation within the Alaska Range suture zone: A polyphase reactivated terrane boundary: Geosphere, v. 15, p. 1066–1101, https://doi.org/10.1130/GES02014.1.
- Trop, J.M., Benowitz, J.A., Kirby, C.S., and Brueseke, M.E., 2022, Geochronology of the Wrangell Arc: Spatial-temporal evolution of slab edge magmatism along a flat slab subduction-transform transition, Alaska-Yukon: Geosphere, v. 18, p. 19–48, https://doi.org/10.1130/GES02417.1.
- Turner, D.L., Triplehorn, D.M., Naeser, C.W., and Wolfe, J.A., 1980, Radiometric dating of ash partings in Alaskan coal beds and Upper Tertiary paleobotanical stages: Geology, v. 8, p. 92–96, https://doi.org/10.1130/0091-7613(1980)8<92:RDOAPI>2.0.CO;2.

- Wahrhaftig, C., 1987, The Cenozoic section at Suntrana, Alaska, in Hill, M.L., ed., Cordilleran Section of the Geological Society of America Centennial Field Guide 1: Boulder, Colorado, Geological Society of America, p. 445–450, https://doi.org/10.1130/0-8137-5401-1.445.
- Waldien, T., 2015, Evolution of a Range-Boundary Thrust in a Strike-slip Fault System: The Late Miocene–Recent Slip History of the McCallum Creek Fault, Eastern Alaska Range, Alaska [M.S. thesis]: Davis, California, University of California–Davis, 121 p., https://search.proquest.com/dissertations-theses/evolution-range-boundary-thrust-strike-slip-fault/docview/1775324372/se-2?accountid=13360.
- Waldien, T.S., Roeske, S.M., Benowitz, J.A., Allen, W.K., Ridgway, K.D., and O'Sullivan, P.B., 2018, Late Miocene to Quaternary evolution of the McCallum Creek thrust system, Alaska: Insights for range-boundary thrusts in transpressional orogens: Geosphere, v. 14, p. 2379–2406, https:// doi.org/10.1130/GES01676.1.
- Waldien, T.S., Roeske, S.M., Benowitz, J.A., Twelker, E., and Miller, M.S., 2021, Oligocene–Neogene lithospheric-scale reactivation of Mesozoic terrane accretionary structures in the Alaska Range suture zone, southern Alaska, USA: Geological Society of America Bulletin, v. 133, no. 3–4, p. 691–716, https://doi.org/10.1130/B35665.1.
- Wessel, P., and Kroenke, L.W., 2007, Reconciling late Neogene Pacific absolute and relative plate motion changes: Geochemistry Geophysics Geosystems, v. 8, Q08001, https://doi.org /10.1029/2007GC001636.
- Wiedmer, M., Montgomery, D.R., Gillespie, A.R., and Greenberg, H., 2010, Late Quaternary megafloods from Glacial Lake Atna, southcentral Alaska, U.S.A.: Quaternary Research, v. 73, p. 413–424, https://doi.org/10.1016/j.vgres.2010.02.005.
- Wilson, F.H., Hults, C.P., Mull, C.G., and Karl, S.M., compilers, 2015, Geologic Map of Alaska: U.S. Geological Survey Scientific Investigations Map 3340, pamphlet 196 p., 2 sheets, scale 1:1,584,000, https://doi.org/10.3133/sim3340.
- Worthington, L.L., Van Avendonk, H.J.A., Gulick, S.P.S., Christeson, G.L., and Pavlis, T.L., 2012, Crustal structure of the Yakutat terrane and the evolution of subduction and collision in southern Alaska: Journal of Geophysical Research–Solid Earth, v. 117, B01102, https://doi.org/10.1029/2011JB008493.
- Yukon Geological Survey, 2020, Yukon Digital Bedrock Geology: Whitehorse, Yukon, Canada, Yukon Geological Survey, http://www.geology.gov.yk.ca/update\_yukon\_bedrock\_geology\_map.html (accessed 19 September 2019).